Geomorphology
November 2020, Volume 369 Pages 107368 (23p.)
https://doi.org/10.1016/j.geomorph.2020.107368
https://archimer.ifremer.fr/doc/00642/75458/

On the termination of deep-sea fan channels: Examples from the Rhône Fan (Gulf of Lion, Western Mediterranean Sea)

Droz Laurence [1, *] , Jégou I. [1], Gillet H. [1], Dennielou Bernard [2], Bez M. [3], Canals M. [4], Amblas D. [4], Lastras G. [4], Rabineau Marina [1]

[1] CNRS, UMR 6538 Laboratoire Géosciences Océan, Institut Universitaire Européen de la Mer, Place Nicolas Copernic, 29280 Plouzané, France
[2] IFREMER, Unité de Recherche Géosciences Marines, CS 10070, 29280 Plouzané, France
[3] Centre Scientifique et Technique Jean Feger, Total, Avenue Larribau, 64018 Pau, France
[4] CRG Marine Geosciences, Department of Earth and Ocean Dynamics, Faculty of Earth Sciences, University of Barcelona, 08028 Barcelona, Spain

* Corresponding author : Laurence Droz, email address : Laurence.Droz@univ-brest.fr

Herve.Gillet@u-bordeaux.fr ; Bernard.Dennielou@ifremer.fr ; Martine.Bez@total.fr ; miquelcanals@ub.edu ; damblas@ub.edu ; glastras@ub.edu ; Marina.Rabineau@univ-brest.fr

Abstract :

The termination of a deep-sea turbiditic channel represents the ultimate sink of terrigenous sediment in the oceans or lakes. Such environment is characterized by rapid slope decrease and by loss of confinement of turbidity currents. It results in the deposition of Channel-Mouth-Lobes that can be separated from the channel mouth by an erosional (scoured) or by-pass dominated Channel-Lobe Transition Zone. Several factors can control the occurrence, extent and morphologic expression of the area such as the slope break angle, the upslope and downslope angle and the mud/sand ratio in flows. Disentangling these factors remains challenging due to the scarcity of outcrops and to the usual faint morphologies and low thickness of deposits. With bathymetric and seismic data we calculated the morphometric parameters of 8 channel-levees and their Channel-Mouth Lobes from the deepest area of the Rhone fan, a mud-sand rich system, and among which the youngest one (called neofan) was deposited at the end of the Last Glacial Maximum between 21.5 and 18.3 ka cal. BP. Emplacement and shape (finger-shaped or pear-shaped bulges) of Channel-Mouth Lobes is controlled by the seabed morphology (adjacent channel-levees and salt diapirs). A less prominent morphology of the neofan is attributed to premature quiescence related to the post sea-level rise sediment starvation. We show that the occurrence and expression of a Channel-Lobe Transition Zone is controlled by the gradient upstream of the channel mouth slope break. The extended Channel-Lobe Transition Zone and detached lobe of the neofan are attributed to the high upslope gradient (0.26°) while the less detached or attached lobes of other channel-levees is attributed to lower upslope gradient (0.13°). We show that scouring and scours concatenation into flutes at the Channel-Lobe Transition Zone is a major driver for the inception of channels and further confinement of turbidity current. For the first time we show that concatenation of

scours in shingled disposition developed an incipient channel sinuosity at this very early stage of channel development. The channel-levee can extend downslope nearly instantaneously by tens of kilometers when isolated nascent channels connect to the channel mouth.

Highlights

► Relative chronology of Late Quaternary Rhône fan channel-levee avulsions ► Evolution of detailed architecture at channel terminations ► Downslope evolution related to high rate of slope gradient changes ► Role of scours in the early formation of sinuous erosional channels

Keywords : Rhone Fan, Turbidite system, Terminal lobes, Geophysics

1. INTRODUCTION

In the long journey of sediment transfer from source to sink, the farthest and deepest sink occurs at the termination of deep-sea turbiditic channels. There, turbidity currents undergo drastic hydrodynamic changes (Komar, 1971), spread out and die out because they lose confinement by levees and lose momentum because of too low gradient. In this context complex sedimentary processes occur. Terminations of turbiditic deep-sea channels are key areas in the partitioning sand in turbidite systems, in sandy systems indeed but also in muddy systems (Piper and Normark, 2001; Pirmez and Imran, 2003; Jégou et al., 2008) and are therefore potential hydrocarbon reservoirs (Piper and Normark, 2001; Zhang et al., 2017).

One striking and ubiquist feature is the occurrence of shifting lobe-shaped bodies referred to as Channel-Mouth Lobe (CML) that show as clusters with a nested compensational stacking pattern reported both in modern and fossil systems regardless of the sediment source type (muddy or sandy) and of the receptacle morphology. Hence, up to five hierarchical units of compensational depositional bodies with increasing thickness and size are commonly described to form clusters named lobe complexes (Deptuck et al., 2008; Prélat et al., 2009; Mulder and Etienne, 2010; Straub and Pyles, 2012). However bodies size and thickness vary and seem controlled by the degree of confinement of the receptacle rather than by the grain size of the sediment (Prélat et al., 2010), though these two characteristics are not independent.

Another striking feature is the frequent occurrence between the channel mouth and the lobes of pervasive erosion in the form of scouring interpreted as a bypass-dominated area and referred to as Channel-Lobe Transition Zone (CLTZ) (Mutti and Normark, 1987). The occurrence of such area controls the connection between the channel-levee and the lobes, which is major concern for the quality of potential hydrocarbon reservoirs (Amy, 2019). When present, a CLTZ is associated to break of slope at the channel mouth and scouring is interpreted as the result of turbidity currents hydraulic jump at the slope break leading to rapid flow expansion and increased turbulence (Wynn et al., 2002a). A CLTZ is however not

always present and its occurrence maybe related to the slope break angle and to the mud-sand amount and turbidity currents efficiency (Wynn et al., 2002a). The question of control by slope and slope breaks remains a matter of debate because recent flume tank experiments have outlined that rather than the angle of the break slope, increased size of a CLTZ is controlled by increased upslope gradient (Pohl et al., 2020), while scouring results from the loss of confinement of turbidity current and resulting flow relaxation (Pohl et al., 2019).

CML and CLTZ are evolving dynamic areas as seen by the aggregation of lobes in clusters both in mud rich and sand rich systems (Twichell et al., 1991; Deptuck et al., 2008; Jégou et al., 2008; Migeon et al., 2010; Prélat et al., 2010; Dennielou et al., 2017). They are also areas of fan development and propagation onto the seabed and accompanied by channel inception. Such a geological process is difficult to image in modern systems owing to the partial overlap of lobes and faint morphologic expression on very deep seas hardly resolved by ship hull mounted acoustic tools and whose details are resolved by deep-tow or autonomous vehicles close to the sea bed (Fildani et al., 2013; Carvajal et al., 2017; Dennielou et al., 2017; Maier et al., 2020). Detailed bathymetric and outcrop based descriptions have outlined the occurrence of erosion and maybe the prerequisite character of erosion and trains of erosional cyclic steps for focusing turbidity currents and initiate accretion of lateral levees (Fildani et al., 2013).

Yet the factors that control the shape, size as well as duration, connection and interaction between channel-levee mouth, CLTZ and CML and their role in fan propagation and channel inception need investigation. In this paper we shed light on the CMLs of the Rhône fan, the second biggest fan in the Mediterranean, categorized as mud-sand rich (Reading, 1991). We investigate the morphometric parameters of 8 recent CMLs, including the youngest one, the neofan, resulting from the channel that developed after the last avulsion near the end of the Last Glacial Maximum (Droz and Bellaiche, 1985; Torres et al., 1997; Bonnel et al., 2005). The opportunity to investigate so many CMLs on the same turbidite system in a geologically short period of time is a great value, as it minimizes the role of external changes and permits

to investigate the role of local factors such as the slope and the maturity of the avulsion on the expression of CMLs.

We examine and discuss the origin of the occurrence of a CLTZ and degree of connection between the channel mouth and the lobes. One aim of the study is to quantify the variability of CMLs size and shape within a mud-sand rich turbidite system and to see how it fits in a broad classification scheme (Prélat et al., 2010). We also aim at understanding the role of external factor such as slope, slope breaks and diapirism on the occurrence and morphological characteristics of CLTZs. In this line we also address the question of channel-levee evolution and maturity ensuing an avulsion and possible control on the expression of CML and CLTZ. Thanks to the exceptional preservation of the CLTZ on the neofan we address the question of channel inception and propagation as well as of sinuosity at a very early stage of inception.

2. GEOLOGICAL BACKGROUND

Due to the wealth of geophysical and sedimentological data acquired in the Gulf of Lion since 1965 (Menard et al., 1965), the Plio-Quaternary architecture of the margin and the sediment sources to the basin are well known (Lofi et al., 2003; Leroux et al., 2014; Rabineau et al., 2014; Leroux et al., 2017). Deep-sea sedimentation since the Pliocene was dominated by gravity processes, i.e. turbidity currents and mass-transport processes (Droz and Bellaiche, 1985; dos Reis, 2001; dos Reis et al., 2005; Jallet and Giresse, 2005; Droz et al., 2006; Jégou, 2008; Dennielou et al., 2019; Badhani et al., 2020) (Fig. 1a).

The outer shelf and slope of the Gulf of Lion are dissected by numerous canyons (Berné et al., 2002a; Berné et al., 2002b; Baztan et al., 2005) that provided pathways to the deep Balearic basin for the Rhodanian and Pyreneo-Languedocian detrital sediments, where they accumulated as turbidite systems since the Plio-Quaternary (dos Reis et al., 2005; Droz et al., 2006). The Rhône Fan, situated in the central part of the Gulf of Lion, is the largest of

135 these turbidite systems, and comprises a 1500 m-thick accumulation of turbidites and mass-
136 transport deposits (Droz and Bellaiche, 1985; dos Reis et al., 2005).
137 The Quaternary Rhône fan is composed of stacked channel-levee systems grouped into
138 three major complexes (lower, middle and upper complexes from the oldest to the youngest,
139 Fig. 1a) partly overlapping each other and shifted westwards. The channel-levee complexes
140 show a basinward divergent architecture (fan-shaped) from the Petit-Rhône Canyon common
141 point source. The upper channel-levee complex extends from the canyon head to its distal
142 limit along about 350 km and laterally up to 150-200 km. Time of initiation remains uncertain
143 and was assigned 200-500 ka (Droz et al., 2006) or 900 ka (Leroux, 2012). Recent seismic
144 correlations from shelf reflectors related to lowstands of 100,000 years cycles (Rabineau et
145 al., 2006) and ground-truthed by drill cores (Bassetti et al., 2008) towards the basin allowed
146 refining the basal age of the upper complex to about 450 ka (Leroux, pers. com.). The fan
147 was fed mainly by alpine inputs of the Rhône River (Molliex et al., 2016; Leroux et al., 2017).
148 Fluvial incision of the shelf occurring recurrently during Late Pleistocene sea-level lowstands
149 (during glacial maxima) is known to have connected the Rhône River outlet and the Petit-
150 Rhône Canyon head through a deep incised valley on the shelf (Torres, 1995; Berné et al.,
151 2001; Berné et al., 2002a; Marsset and Bellec, 2002).
152 Several huge mass-transport deposits (MTDs) described on the Gulf of Lion and Catalan
153 margins (Droz and Bellaiche, 1985; Bellaiche et al., 1986; Gaullier et al., 1998; Lastras et al.,
154 2004; Droz et al., 2006; Lastras et al., 2006; Jégou, 2008; Dennielou et al., 2019; Badhani et
155 al., 2020) attest the importance of repeated periods of slope instability during the Quaternary.
156 The youngest of these MTDs (Western and Eastern Upper MTDs) rest unconformably on
157 both sides of the recent channels of the upper complex and were both emplaced during the
158 last lowstand between 22-20 ka BP (Dennielou et al., 2019; Badhani et al., 2020) (Fig. 1a).
159 Following this episode of instability, the Rhône fan underwent a last channel avulsion to the
160 west that led to the abandonment of the southern part of the fan and diverted the deposition
161 in a more proximal part of the fan, to develop the so-called neofan located above the
162 Western MTD. AMS radiocarbon dating indicates that deposits of sediment spillover from the

neofan channel stopped at 18.3 cal. ka BP (age calibrated after Bonnel et al., 2005), i.e. during the onset of the post-glacial sea-level rise (Bonnel et al., 2005; Jégou, 2008). Turbiditic activity persisted upstream of the neofan avulsion until 16.5 cal. ka BP (Lombo-Tombo et al., 2015) and in the western part of the Gulf of Lion during the Holocene (Droz et al., 2001; Bonnel et al., 2005; Dennielou et al., 2009) possibly linked to strong hydro-sedimentary dynamics on the outer shelf (Bassetti et al., 2006) and dense water cascading processes in the canyon heads (e.g. Canals et al., 2006; Gaudin et al., 2006; Palanques et al., 2006).

Seafloor mounds related to subsurface salt diapirs influence the topography over a wide area in the distal parts of the fan (Fig. 1b). Diapirs, which result from movement of the Messinian salt during deposition of the Plio-Quaternary sediments, deform the seafloor with mounds up to 250 m high, and show a great variability in plan-view shapes (either rounded or N-S to NNE-SSW to E-W elongated) and width (from some hundreds of meters to several kilometers).

3. DATA AND METHODS

In this paper, we document the first complete chronology of the development of the distal Late Quaternary Rhône fan. Based primarily on high- and very high-resolution bathymetric data and sub-bottom profiles (SBP) we show in detail the morphology, seismic facies, architecture and relative chronology of the distal channels and CMLs extending south of latitude N42°15'. The description of the neofan relies on new data but also takes into account previously published work (O'Connell et al., 1991; Kenyon et al., 1995; O'Connell et al., 1995; Torres et al., 1997; Droz et al., 2001; Wynn et al., 2002a; Droz et al., 2003b; Bonnel et al., 2005; Jégou, 2008). The description of the channels and terminations of channel-levee-lobe systems older than the neofan is entirely based on unpublished data.

This study is mainly based on EM300 multibeam bathymetric and backscatter data and sub-bottom profiler (SBP) seismic data acquired during PROGRES 2003 cruise (Droz, 2003;

190 Droz et al., 2003b) as part of EUROSTRATAFORM European Program. Additional EM12
191 bathymetric and SBP data acquired during SARDINIA cruise (Aslanian et al., 2006), deep-
192 towed MAK-1M side scan sonar data and 5 kHz sub-bottom profiles acquired during cruise
193 TTR14 (UNESCO Training-Through-Research program) (Kenyon et al., 2006) complement
194 the PROGRES data.

195 ***3.1. Bathymetric data***

196 The EM300 bathymetric data have been combined to produce a 50 m grid spacing Digital
197 Terrain Model (DTM) in the neofan area at water depths down to 2000 m. For deeper water
198 depths the grid spacing of the DTM is 100 m.
199 In order to enhance the visualization of the low-relief terminal areas of the channels, the
200 PROGRES DTM was processed (Fig. 2) with the SonarScope software developed at Ifremer
201 (https://www.flotteoceanographique.fr/en/Facilities/Shipboard-software/SonarScope). The
202 overall regional slope was subtracted from the DTM (Fig. 2a) by using a polynomial surface
203 (Fig. 2b) corresponding to the mean water depth surface of the southern terminal reaches of
204 the fan. The resulting de-trended DTM (Fig. 2c, d), herein called relief map, delineates zones
205 that are higher and lower than the mean water depth surface (see Picot et al., 2016, for
206 further details on the method).

207 ***3.2. MAK-1M side-scan sonar data***

208 Side-scar sonar data on the neofan were recorded from a deep-towed platform embarking a
209 MAK-1M 30 kHz side-scan sonar. Data were acquired at 2.5 knots, about 100 m above the
210 seafloor, allowing a total swath range of 2 km with a resolution varying between 7 and 1 m
211 across track and along track respectively. Data consist of 9 N-S profiles positioned at the
212 apparent termination of the neochannel, from N42°02 and N41°41 (Fig. 1b).

213 ***3.3. Very high-resolution sub-bottom profiler data***

214 Most of the very high-resolution sub-bottom profiler (SBP) data were acquired from the hull-
215 mounted system during the PROGRES cruise (Droz, 2003) at a mean speed of 8 knots in the

chirp configuration (1.8-5.0 kHz). Data were processed using a simple correlation algorithm (matched filter) followed by an envelope representation (Hilbert transform). SBP data consist mostly in SW-NE strike profiles with 4 to 8 km of line spacing, crossed by 4 dip lines. SBP profiles allowed the seismic characteristics (facies, overlapping pattern and relative stratigraphy) of depositional bodies to be described. However, in the most distal areas with numerous small depositional bodies intercalated between salt diapirs (Fig. 1), the large spacing of lines (8 km) did not allow robust stratigraphic correlations.

Our study also benefited from hull-mounted chirp data acquired during the SARDINIA cruise (Aslanian et al., 2006) and MD114 cruise (Labeyrie et al., 2003) and from a 5 kHz sub-bottom profiler installed in the deep-towed MAK-1M platform acquired at 2.5 knots during the TTR14 cruise (Kenyon et al., 2006).

4. RESULTS

4.1. Imaging of faint morphologies of CMLs

The corrected relief map (see Section 3.1, Fig. 2) proved to be a useful tool to enhance subtle topography that characterizes distal parts of fans. This method helped to overcome the difficulties in correlating narrow seismic units across a sometimes widely spaced seismic grid (especially to the southeast) lacking transverse profiles, and allowed the downstream extension of the channels to be defined. It also shows elongated topographic convexities called morphological bulges. From the relief map, we were also able to visualize and characterize small topographic features, such as 10 m deep scours (in > 2500 m water depth). However, caution must be taken when interpreting morphological bulges in terms of depositional bodies. The morphological bulges traced from the relief map are positive relief features compared to a regional slope surface. The existence of a bulge is therefore linked to a balance between inherited topography and sediment thickness. Where the thickness is lower than the inherited topographic low between previous units, the deposition is not really

visible as a bulge. Although this is an infrequent situation at the most distal part of the fan, seismic interpretation is necessary to ensure the limit of the depositional units.

4.2. Channel-levee network

4.2.1. Planform morphology and channel chronology numbering

The plan view of the channel network of the Rhône fan shows a basinward diverging, fan shape pattern (Figs. 3, 4a) as for many modern mostly unconfined deep-sea fans on passive margins, such as the Danube Fan (Popescu et al., 2001), the Amazon Fan (Jégou et al., 2008) or the Congo Fan (Picot et al., 2016).

Based on the plan view morphology and on the geometries observed on SBP, 15 main avulsion nodes with a marked plan view morphological expression and 24 avulsion nodes with a faint morphological expression have been identified. Main avulsion nodes are numbered from 1 to 15 from the oldest to the youngest (Fig. 4). A four-order hierarchical classification of channels developed after avulsion is proposed based on the plan view clustering (Fig. 4 and 5). Thus the Rhône fan channel network is composed of 8 channel-levees clusters that diverge from the Rhône Valley (Fig. 3). Channel-levees clusters, partially overlapping each other, have developed after 7 main avulsions and have been labelled 7 to 1 from old to young with the youngest labelled N for neochannel (Figs. 3, 4d, 5a). Further downstream, except for channels 5, 1 and N, these channel-levees have undergone second to fourth order avulsions (Fig. 4d), giving rise to a complex network of distributaries. Channels 7 to N with their distributaries form “groups of channels”, so that eight groups of channels characterize the distal fan.

It is noteworthy that avulsion nodes of channel groups 7 to 1 (yellow dots in Figs. 4 and 5) continuously stepped basinwards (Fig. 5b), reaching a maximum distance for avulsion node 14 (from channel 2 to channel 1). Consecutively, the neofan shifted abruptly at the most upfan location (avulsion node 15, from channel 1 to N). This continuous basinwards

267 migration of main avulsions is balanced by downstream-upstream shifts of second order
268 avulsion nodes (black dots in Figs 4 and 5) defining a higher order of depositional
269 prograding-retrograding trend in an overall prograding pattern.
270 The channels show different morphological characteristics possibly as a function of their age,
271 duration or maturity. To the east, channels 7 to 1 are up to 84 km long, highly sinuous and
272 have developed between salt diapirs and salt walls (Figs. 1, 4a). Depressions between
273 diapirs are linear normal fault systems reaching the seafloor and related to salt tectonics. The
274 vertical offset of faults reach several tens of meters, up to 50 m. These abrupt topographic
275 variations have affected the evolution of the channels by creating obstacles. Basinward
276 beyond the salt domes, channels diverge and become straighter toward the Balearic Basin,
277 at least until latitude N40°10' as indicated by still visible portions of channels in this area
278 (black lines in Fig. 4a).
279 In contrast, the neochannel to the west is short, with a length of 20 km from the avulsion
280 node. It diverges from the abandoned main channel (stacked channels 7 to 1, Fig. 3c) in a
281 NNE-SSW direction and is rather straight until it bends towards the south, while its imprint on
282 seafloor morphology gradually diminishes, becoming so faint that it is no longer resolved.
283 The morphology of the abandoned main channel (AMC used by channels 7 to 1, Fig. 3c),
284 below the neochannel avulsion node is blurred over about 20 km because of later sediment
285 infill (Fig. 4b). Droz and Bellaiche (1985) indicate that the infill was due partly to mass-
286 movement deposition inside the channel that resulted in its obstruction and probably
287 generated the westward neochannel avulsion. Further infill was by fine-grained turbidites
288 from flow stripping and overbanking from the neochannel until 18.3 cal. ka BP. Hemipelagic
289 and/or pelagic deposits probably also contributed to the healing of the relief. Further
290 downstream, the abandoned main channel has developed to the S-SE and maintained a
291 clear topographic expression on the seafloor with a clear sinuous incised channel (Fig. 4b),
292 despite hemipelagic deposition since its abandonment at ca 20 cal. ka. The channel floor is
293 perched 200 m above the surrounding seafloor (Fig. 4c, bathymetric profile A).

294 *4.2.2. Channel gradients*

295 The along-channel bathymetric profiles (Fig. 6) show that, prior to abandonment, channels
296 2c1, 2bn, 2b1, 2a1 and 1 were at equilibrium state (parabolic estimated channel floor profile,
297 black dashed line in Fig. 6a). In contrast, the Rhône Valley and neochannel depth profiles
298 are irregular and comprise a marked knick-point (pink dot in Fig. 6) upstream of the avulsion
299 node (Torres et al., 1997; Bonnel et al., 2005; Jégou, 2008) where channel slope changes
300 from 0.52° to 1.42° according to Jégou (2008), indicating that retrogressive erosion inside the
301 Rhône Valley followed the avulsion and was still active until the neofan was abandoned at
302 18.3 cal. ka (age calibrated after Bonnel et al., 2005).
303 The retrogressive erosion reached 120 m of vertical amplitude and propagated 25 km
304 upstream the avulsion node at an average rate of ca 10 km/ka considering the duration of the
305 neofan. This is one to two orders of magnitude slower than knick-points migration velocities
306 measured in presently active channels (Guiastrennec-Faugas et al., 2020; Heijnen et al.,
307 2020) but it is risky to compare changes at annual and millennial time scales. Downstream of
308 the knick-point, the neochannel thalweg slope is rather smooth with a convex-up, near-
309 equilibrium profile and slope gradients decreasing from 0.49° to 0.26° until the point where
310 the neochannel is not any more visible.

311 *4.2.3. Seismic facies and architecture*

312 Strike oriented SBP lines across the channel-levees systems reveal typical transparent to
313 stratified wedge-shaped seismic facies in levees and high-amplitude chaotic channel fills that
314 create acoustic masks (Fig. 7). The channel-levee systems rest locally on high-amplitude
315 units. By comparison with high-amplitude reflection packets (HARPs) that characterize
316 avulsion lobes in the Amazon Fan (Pirmez and Flood, 1995; Pirmez et al., 1997; Mansor,
317 2009; Ortiz-Karpf et al., 2015) and in other fans (e.g. Flood et al., 1991; Popescu et al., 2001;
318 Droz et al., 2003a; Schwenk et al., 2005) and considering their locations close to the avulsion
319 nodes, these high-amplitude units are interpreted as avulsion lobes, over which the channel-

levee systems have aggraded and prograded without any evidence of incision into the HARPs

The neochannel (Fig. 7a) is bordered by external levees up to 40 ms twt (~ 30 m) thick (Bonnel et al., 2005) and 19 km wide that rest on a 30 ms twt (~ 20 m) thick high-amplitude avulsion lobe. Torres et al. (1997) showed that the southern limit (more precisely the 10 ms twt seismic thickness, i.e. the resolution of the high-resolution seismic data) of the neofan's HARPs is restricted to Lat. N 41°40. A 2 m thick hemipelagic drape, indicative of the abandonment of the neofan is observed on seismic profiles (Fig. 7a) and at the top of a core that sampled the external side of the right neofan levee (core MD99-2344 in Bonnel et al., 2005). The channel-levee systems 7 to 1 are 30 to 60 ms twt thick (20 to 45 m), including the basal high-amplitude avulsion lobes, that is 10-15 ms twt thick (8-10 m) and can locally contribute to nearly half of the total thickness of the system (Fig. 7b-c). Lateral extensions of these channel-levee systems are not measurable because salt domes interrupt the continuity of the deposits. A lateral extension of about 30 km has been estimated for system 4b (Fig. 7c).

4.3. Channel mouth areas

The morphology of the channel mouth areas (Figs. 8, 9) is very subtle with relief amplitude generally not in excess of 10 m and very low average slopes (0.2°-0.1°). The bathymetric expression of morphological features is partly a function of the thickness of the post-abandonment sediment cover (i.e. hemipelagic deposition and/or turbiditic overspill deposit from younger channels) and therefore of the age of the depocenters. The resolution of the DTMs (50 m for the neofan area and 100 m for older depocenters, see Section 3.1) is another factor hampering a clear assessment of the topographic expression. Therefore, the young neofan shows the morphological features with the highest resolution, and the following description of the morphological features at channel mouths will be based on the observations of the neochannel mouth.

347 *4.3.1. General morpho-structural overview of channel mouth areas*

348 The neofan channel-levee system progressively tapers and transitions to a 5 km long smooth
349 area (Fig. 8a-b) where the seafloor is free of channels. Westward of this smooth area, the
350 seafloor is characterized by numerous, mostly symmetrical depressions (< 2 m deep) (giant
351 scours in Fig. 9a) visible on SBP cross lines (Fig. 9a). The seismic facies in this area is
352 transparent, with some discontinuous reflectors at the top, whose exact origin is unknown. A
353 comparison with upstream stratified and laterally continuous overbank deposits (Fig. 7a),
354 suggests that these deposits are different, and related to lobe deposits rather than to levees.
355 The lack of seismic indicators of channel-levee in this area is consistent with the end of
356 channel incision (Fig. 8a-b) and suggests that the sediments exiting the neochannel
357 bypassed (sensu Stevenson et al., 2015) this area to be deposited basinwards.
358 About 4 km downstream of the sediment bypass dominated area, the seafloor is
359 characterized by pervasive erosional features (Figs. 8, 9b) of two types, i.e. scour marks and
360 elongated channel-like features that are not connected to the neochannel. The channel-like
361 features incise into an almost transparent seismic facies with some discontinuous reflectors
362 forming wedge-shaped seismic bodies (Fig. 9b), less than 20 m thick and apparently thinning
363 outwards from the erosive channel axes. Further south, i.e. 30 km from the neochannel
364 mouth, erosional features are not observed and the seafloor is smooth and generally free of
365 distributive channel and shows deposits in the form of 10 m thick wedge-shaped seismic
366 units with highly reflective top surface (Fig. 9c).
367 The distal portions of channel groups 1 and 2 are characterized on the relief map by positive
368 reliefs (called bulges) surrounding channels and channel mouths, delineating elongated
369 bulges, either narrow (2cn, 2c, 2b1), or pear-shaped (2bn, 2b2, 1) (Fig. 10a). In upstream
370 portions, bulges are 7 to 20 km wide, and a central sinuous channel is generally identifiable
371 (channels 2c and 1, Fig. 10b) or inferred (channels 2b and 2a, Fig. 10b). The downstream
372 portions of the widest bulges have widths up to 43 km (bulge $2b_n$, Fig. 10b). The topographic
373 bulges of channel groups 1 and 2 correspond to seismic bodies evolving downstream from
374 channel-levee systems up to 25 ms twt (~ 19 m) thick, with well-identified stratified to

375 transparent external levees (Fig. 11a), to wedge-shaped seismic sub-units made of a
376 combination of chaotic facies with very high-amplitude reflectors, and transparent facies
377 (Fig.11b-d).
378 The seismic analysis provided some clues to establish a relative chronostratigraphy for the
379 identified seismic sub-units (Fig. 4d). However, wedge-shaped sub-units are numerous and,
380 except for bulges 2b and 2a, due to the low penetration of SBP data and the scarcity of
381 transverse profiles to correlate these small sub-units, the chronostratigraphic relationships
382 between the seismic sub-units remain incomplete and/or uncertain. The bathymetric bulges
383 2b and 2a are sub-divided into at least 2 to 4 successive seismic sub-units, 8 to 20 ms twt (~
384 6 to 15 m) thick and generally thinning downfan (Figs. 10, 11). Some evidences of back-
385 stepping geometries are observable at the distal part of this system (Fig. 12, north-western
386 part of the profile).
387
388 *4.3.2 Detailed seafloor morphology*
389 The Rhône fan terminal areas are characterized by erosional features (scours) and
390 depositional elements (wedge-like features) that can be spatially separated or coeval. In the
391 neofan, they are clearly linked to changes in slope (Fig. 6). Such erosional and depositional
392 bedforms are also observed in the terminal parts of channel groups 2b to 1 (Fig. 10).
393 Longitudinal slope analysis for bulges 2c1 to 1 (Fig. 13) shows small gradients (average ~
394 0.12°, Fig. 6a), decreasing from 0.18° upstream to 0.09° downstream where the fan merges
395 with the flat Balearic abyssal plain. Scours and unconnected channels are identified on
396 slopes (0.13° to 0.10°, Fig. 13) lower than those of the neofan (0.21°, Fig. 6). The
397 bathymetric profiles of channels 2b to 1 and their lobate extension show more regular
398 decrease of slopes than the neochannel, with no major slope break, even at the avulsion
399 nodes. Note that slope of these fossil channel-lobes is measured from straight lines at the
400 channel axes and do not account for the sinuosity of the channels. Consequently, calculated
401 slope of the old channel-lobes tends to be overestimated except in the terminal parts where
402 channels are mostly straight.

403

404 4.3.2.1 Scour marks

405 Downstream the neofan and neochannel numerous scour marks are observable on
406 bathymetric data (Fig. 6). The scours are characterized by asymmetrical dip profiles, with
407 steeper updip flanks. On strike profiles they are either symmetrical or asymmetrical (S or A,
408 respectively, on Fig. 14). The scours on the neofan occur on a mean slope of 0.21° (Fig. 6)
409 and show various dimensions. On the right outer levee of the neochannel coalesced giant
410 scours, 10-30 m deep, 1-2 km wide and 1-5 km long scours (Figs. 8b, 14a) previously
411 described by Kenyon et al. (1995), Bonnel et al. (2005), Jégou (2008) and Dennielou et al.
412 (2009) have an updip flank mainly oriented NW-SE. Smaller scours, 5-10 m deep, less than
413 500 m wide characterize the area of the neofan located off the termination of the neochannel
414 (Figs. 8b, 14a). The updip flanks of small scours are mainly oriented E-W, i.e. more or less
415 transverse to the neochannel termination. They evolve downstream to smaller triangular
416 chevron-like scours that progressively disappear southwards (Fig. 14a).
417 Scour marks are also observed at the top of bulges 1 and 2 (Fig. 14d) in the form of several
418 meters deep depressions that are generally symmetrical but can also be asymmetrical in
419 some cases with flanks sloping at different angles (strike lines in Fig. 14d). The deepest
420 depressions are 5 m deep and 300 m wide, but most often the width of these features is 100-
421 200 m, regardless of the symmetry. Scours on bulges are hardly resolvable on SBP sections
422 where they are mainly expressed as hummocky areas (Figs. 10b, 11b).

423

424 4.3.2.2 Channel-like linear erosional features

425 At the distal part of the by-pass area, at the termination of the neochannel, in an area of low
426 slope gradient (~ 0.2°), SBP strike lines show 10 m deep erosive features (Figs. 14a, 15)
427 incising an almost transparent substrate, with few discontinuous reflectors. In plan-view,
428 these erosional features are elongated (up to 15 km long) and narrow (generally less than
429 500 m wide) channel-like features (called Ch1 to Ch3, without any chronological order

430 inferred). A fourth channel-like feature (Ch4, Fig. 15a) is located upslope at the outer bend of
431 the first bend of the neochannel.
432 High-resolution 5 kHz SBP profiles fail to reveal the relative age of these channel-like
433 features with regard to the neochannel, but show that these conduits do not develop external
434 levees and appear as purely erosional features. Detailed topographic analysis of the
435 channel-like features (Fig. 15b) allows numerous E-W oriented < 500 m wide, semi-circular
436 scours to be identified along their length, similar to those of the small scours field. On very
437 high-resolution MAK-1M side-scan sonar, these scours show downchannel facing headwall
438 scarps prolonged by elongated erosional lows. On MAK-1M 5 kHz SBP, the scours are
439 symmetrical on transverse cross sections (s1 and s2 in Fig. 16b, c) and asymmetrical with a
440 steeper headwall when longitudinally crossed (s3 and s4 in Fig. 16b, c). The maximum depth
441 of the scours is 14 m at the Ch2 channel head (Fig. 16b), decreasing to 11 m at the southern
442 part of Ch2 (Fig. 16c). Because of their shape and size, these erosion features can be
443 named megaflutes (Lonsdale and Hollister, 1979; Elliott, 2000; Kane et al., 2009). Changes
444 in the channel Ch2 direction are controlled by offsets of the megaflute clusters (about 200 m
445 wide).
446 In addition, MAK-1M mosaic reveals NE-SW to NNW-SSE lineations (Fig. 16a) inside the
447 head of Ch2 and outside this channel, especially on its right hand side. These lineations
448 slightly diverge downslope from an area that could be the outer part of the first bend of Ch1,
449 while Ch2 appears to be superimposed to them.
450 On the morphological bulges and wedge-shaped seismic units related to channels 1 and 2
451 (Figs. 11b, 12), small channels, 7 m deep at maximum, also appear to be unconnected to the
452 main feeder channel of the bulge (Fig. 10). Most of these small, unconnected distributaries
453 appear on seismic lines as erosional features at the top of the units and could correspond to
454 channel-like features similar to those identified on the neofan. However, in contrast to the
455 neofan, the unconnected channels show frequent evidences of associated small external
456 levees, possibly made of coarse-grained deposits owing to their high amplitude seismic
457 facies (channel 2a1 in Fig. 12).

458

459 4.3.2.3 Depositional features

460 The distal part of the neofan, downsteam of the chevron-like scours, is characterized by a
461 very smooth topography on a mean slope of 0.13° (Fig. 6). The seismic profile provided in
462 figure 9c shows wedge-shaped transparent seismic bodies with highly reflective top surface,
463 less than 7 m thick and 5 km wide, and irregular rounded top morphologies and flat bases.
464 Jégou (2008) identified a total of 11 of such seismic bodies with mean thicknesses of 10-15
465 m (minimum few meters and maximum 45 m) in the neofan and extended the distal limit of
466 the neofan near N40°45, i.e. about 160 km from the neochannel bifurcation point. Terminal
467 areas of morphological bulges 1 and 2 are characterized by similar wedged-shape seismic
468 units (Figs. 11b-d, 12), with comparable seismic facies (combination of high amplitude
469 chaotic facies and transparent facies) and sizes (see Table 2). The most superficial wedge-
470 shaped units are 15 ms twt (~ 10 m) thick upfan (bulge 2b, Fig. 11b) with a clear tendency to
471 thin downfan (7 ms twt, i.e. ~ 5 m for bulge 2b1 in Fig. 11c). Several older and buried wedge-
472 shaped units can be identified on SBP data, but due to loss of penetration in these probably
473 coarse-grained environments an accurate thickness cannot be constrained.

474

475 **5. DISCUSSION**

476 ***5.1. Significance of morpho-sedimentary domains***

477 The main geometrical characteristics of morpho-sedimentary domains are summarized in
478 figure 17 and Table 1. The Rhône fan morphological bulges extend for significant distances,
479 i.e. 92 km to 158 km, and contribute from 25% to 43% of the 370 km total length of the fan
480 (Fig. 17, Table 1). Three morpho-structural domains can be identified from upstream to
481 downstream, which are well expressed in the western young neofan, and tentatively
482 recognized in the eastern older and more distal bulges.

In domain 1, depositional processes are dominant in the form of aggradational, up to 30 m thick channel-levee systems that have developed upstream on top of avulsion lobes (HARPs) (Flood et al., 1991; Lopez, 2001; Bonnel et al., 2005) close to the avulsion nodes. Erosional processes are dominant in domain 2, in the form of 10 to 30 m deep erosional features at different degrees of evolution (scours and slightly sinuous channel-like features). These erosional features are interpreted as the result of flow transformation associated with a break of slope and are commonly described in transition areas between well-defined channel-levees and well-defined lobes (CLTZ) (Mutti and Normark, 1987; Wynn et al., 2002a; Brooks et al., 2018). In domain 3, depositional processes dominate on a nearly flat seafloor in the form of stacked 10 m thick (exceptionally 45 m thick) wedge-shaped, possibly channelized seismic units, interpreted as Channel-Mouth Lobes.

The bypass and erosion dominated domain 2 is well-constrained and well developed in the neofan at the end of the neochannel. The exceptional preservation of the erosion marks on the seafloor points to a very abrupt sediment starvation related to the last sea level rise and disconnection of the Rhône River and the Petit-Rhône Canyon (see Section 5.2). Conversely, domain 2 seems poorly developed or absent at the eastern channel terminations. However, the bathymetric expression of the CLTZ was possibly altered by subsequent burial.

Plotting the maximum width versus maximum thickness of domain 3 for channels N, 1, 2a1, 2b1 and 2bn (measurements provided in Supplementary Material) allows referring to domain 3 as unconfined lobes of Prélat et al. (2010) classification (Fig. 18a). This is confirmed by plotting the aspect ratio (length/width) to the maximum thickness/area of these domains (see Supplementary Material for surface calculation). Maximum thickness/area ratio is ~ 10^{-5} (Fig. 18b) similar to that of unconfined lobes of Tanqua Karoo, Amazon and Congo fans with an average aspect ratio of 2.8 (1.9 to 5.8) (Prélat et al., 2010). These results confirm our hypothesis that the morphological bulges of domain 3 can be interpreted as lobes.

5.2. Controls on avulsions

Channel avulsion is a major process in the development of deep-sea fans. It is admitted that the occurrence and location of avulsions is a natural consequence of the development and growth of a channel-levee that cannot indefinitely increase. Therefore avulsion can be controlled by external (sea level and climate changes and consequences on type and quantity of sediment input to the fan) and internal (slides, breaching, spillover processes, thalweg aggradation) forcings that are most of the time entangled and is, like for slope stability processes, a combination of preconditioning factors and trigger mechanisms (see review in Kolla, 2007). On the Rhône fan distal reaches the lack of chronological constrain for channel-levees 7 to 1 prevent to conclude on the external factors that controlled avulsions and their continuous basinward migration (Fig. 5b). One can argue that their emplacement and development were most probably autogenic though slightly controlled by diapirs growth. On the other hand, it is noteworthy that avulsion of the neochannel is remarkably different as it occurred in a very up-dip position on the flank of the Rhône Valley and that the neofan have developed on a higher slope gradient (Fig. 6). The emplacement of the neofan is concomitant with two major external events that could explain the trigger of the avulsion. The neofan has developed on top of a voluminous mass-transport deposit, the Western Mass Transport Deposit (WMTD), that emplaced between 21.5 and 19.9 ka cal BP (Dennielou et al., 2019) and that is deeply incised by the neochannel. Interestingly, the avulsion node lies right above one of the headscars related to the slide, suggesting a causal relationship between the slide and the avulsion. This hypothesis is supported by the fact that external flanks of the Rhône valley, both to the west and to the east, show several massive headscars related to these Last Glacial Maximum (LGM) slidings (Dennielou et al., 2019; Badhani et al., 2020), that nearly reached the inside of the valley and the thalweg, creating favorable conditions for breaching, crevasse splay and eventually channel avulsion (Torres et al., 1997). A similar process was suggested for triggering an avulsion on the Magdalena Fan (Ortiz-Karpf et al., 2015).

537 The neofan was emplaced during the LGM, a period of maximum sediment accumulation on
538 the Rhône fan (Lombo-Tombo et al., 2015), before the last sea level rise and a sediment
539 starvation. High sedimentation rates in the valley were also characterized by coarser
540 deposits (Lombo-Tombo et al., 2015) that could have increased the thalweg aggradation and
541 lead to increased turbiditic overflow and diversion of turbidity currents. Several evidences of
542 levee erosion related to flow spillover are found upstream the neofan (Droz et al., 2001;
543 Bonnel et al., 2005), supporting the hypothesis that several areas of enhanced lateral
544 spillover were potential candidates for channel avulsion. In the same line, thalweg blocking
545 by sliding of channel inner flank and also possibly related to enhanced accumulation has
546 been also invoked for the neochannel avulsion trigger mechanism (Droz and Bellaiche,
547 1985).
548

549 ***5.3. Mature versus immature channel avulsions***

550 The successive changes of architecture, size and topography of domains 2 and 3 of bulges 1
551 and 2 are similar to those observed on the neofan (Table 2).
552 The channel avulsion that formed the neofan occurred in a more proximal position than those
553 of eastern channels 2 to 1 (Fig. 5b), and consequently the neochannel is characterized by
554 much higher along-channel gradients (0.26° to 0.13, Fig. 6). It is also characterized by a
555 major knick-point upstream of the avulsion node indicating that retrogressive erosion did not
556 result in the establishment of a new equilibrium profile, and that the neochannel was at an
557 immature stage when it was abandoned. This suggests that the ca. 2-3 kyr duration of the
558 neofan was insufficient to establish the equilibrium profile in the neochannel after the
559 avulsion. In contrast, avulsion of channels 7 to 1 occurred in more distal positions and
560 channels developed on smaller along-slope gradients (0.15° to 0.09°, Fig. 13). No along-
561 channel knick-point or significant breaks in slope are observed in channels 2c to 1, even
562 close to avulsion nodes, indicating that these channels had probably reached an equilibrium
563 profile when they were abandoned. The distal occurrence of these avulsions, i.e. on smaller

564 slopes, probably favored a rapid establishment of the equilibrium profile and therefore
565 durations longer than the neofan duration are not necessarily needed. However, the
566 existence of small external levees associated with unconnected channels of lobes 2 (Fig.
567 12), which do not exist in the neofan, suggests that these unconnected channels had
568 sufficient time to become permanent pathways for turbidity currents and to build external
569 levees. This leads us to envisage that the eastern channels-lobes 7 to 1 were more mature
570 than the neofan when they were abandoned. This is also suggested by the sinuosity of the
571 channels that supports their maturity as seen in other turbidite systems (e.g., Peakall et al.,
572 2000; Babonneau et al., 2002; Deptuck et al., 2003). Durations of turbiditic lobe activity are
573 rarely reported in literature. The duration of the neofan, between 1.2 and 3.2 kyr is inferred
574 from the age of its onset on top of the WMTD, between 19.9-21.5 ka cal. BP (Dennielou et
575 al., 2019), and the post-seal level rise sediment starvation at 18.3 ka cal. BP (age calibrated
576 after Bonnel et al., 2005). Migeon et al. (2010), indicate duration longer than 2.5 kyr for the
577 Nile Fan terminal lobes. In contrast, in the Amazon Fan, Jégou et al. (2008) estimated to 0.6
578 kyr the duration of individual lobes constituting the youngest lobe complex, whereas Picot
579 (2015) inferred highly variable durations of channel-lobes systems in the Congo Fan, with the
580 youngest lobe of the last lobe complex being deposited during 0.46 kyr. These disparities
581 suggest that channel and lobe durations are highly variable and probably relate to numerous
582 controlling factors, e.g. sea-level and climate controlled sediment input, frequency and
583 magnitude of flow, loci of avulsions, accommodation conditions related to previous
584 depositional and mass-transport episodes and transport capacity of turbidity currents.
585 However this comparison with duration of other channel-levee-lobe systems is challenging
586 considering that a common definition of lobes is not provided in these papers.
587

588 ***5.4. Controls on bulges emplacement and sedimentation***

589 The elongated and narrow or pear-shaped (Fig. 17) planforms of the Rhône fan bulges
590 (domains 2 and 3), and the compensational stacking pattern of seismic units (Figs. 11, 12)

591 support an interpretation that their emplacement was controlled by topographic
592 compensation through the restricted available space. This is obvious for seismic unit 2b1 and
593 2bn (Fig. 11) where sub-units have a clear compensational architecture. The neofan also
594 clearly shows a topographic confinement by the older Rhône fan to the east and the WMTD
595 and deposits from the Catalan channels to the west (Fig. 17). A compensational stacking
596 pattern is also shown by the alternative eastward and westward migrations of the sub-units
597 (violet dashed arrows in figure 17). However, besides this compensational growth pattern,
598 CMLs 2b to 1 and N have morphometric parameters compatible with the unconfined lobes of
599 (Prélat et al., 2010) (Fig. 18), suggesting that topographic confinement is not the principal
600 controlling factor of the growth pattern.
601

602 ***5.5. Channel-Lobe Transition Zone: characteristics and occurrence***

603 In turbidite systems, channel-lobe transition zones (CLTZ) are critical areas where turbidity
604 currents undergo hydro-sedimentary changes associated with breaks of slope and loss of
605 confinement (Wynn et al., 2002a; Dorrell et al., 2016; Pohl et al., 2019). CLTZ are dynamic
606 areas evolving through time (Brooks et al., 2018) and are commonly bypassed by sediments
607 and characterized by patchy coarse deposits, abundant erosional features such as scours
608 and (coarse-grained) sediment waves (Wynn et al., 2002b; Macdonald et al., 2011; Shaw et
609 al., 2013; Hofstra et al., 2015).
610 Domain 2 of the recent Rhône neofan is interpreted as a CLTZ because of the presence of
611 multiple erosional features which coincides with an abrupt slope break in the prolongation of
612 the neochannel (Wynn et al., 2002a).The more distal domain 3, free of erosional features,
613 could therefore be interpreted as a detached lobe(sensu Mutti and Normark, 1987; Van der
614 Merwe et al., 2014).
615 In channel-lobes 7 to 1, domain 2 (hummocky scoured seafloor, Fig. 17a) are observed only
616 at the mouth of channels 1, 2a1, 2b1, 2cn (Supplementary Material and Fig. 17a), and are
617 generally less extended longitudinally (17-26 km, exceptionally 39 km for bulge 2a1,

618 Supplementary Material) than on the neofan (40 km). This striking difference may come from
619 lower resolution of the DTM in this area but may also be related to real morphological
620 differences between these sites. Hummocky morphologies (Figs. 11b, 12b), interpreted as
621 scour fields, do not appear to be linked to significant slope breaks (slope decreases
622 progressively from 0.15° to 0.09°) and the average slope of 0.12° is similar to that of the
623 neofan CML (0.13°). Moreover, we do not identify a sediment bypass-dominated zone at the
624 end of channels 2 and 1. Unless this absence is related to post-avulsion modifications, this
625 could indicate that the domains 2 and 3 of eastern lobes formed attached lobes (Wynn et al.,
626 2002a) where scouring may also occur.
627 Our results show that drawing a universal model for the occurrence and expression of a
628 CLTZ is challenging because these can even change in space and time in a given fan. Two
629 key parameters, generally considered as control factors, are the composition of flow (muddy
630 versus sand rich) and channel mouth slope break (Wynn et al., 2002a). Slope evolution
631 along the terminal parts of channels appears indeed as a strong topographic control.
632 Domains 1 (channel-levee) to 3 (CML) of the neofan show a clear link with slope breaks.
633 Although slope is very low (0.26° to 0.13°), the rate of change (decrease) is high, i.e. 19 %
634 from aggradational channel-levee (0.26°) to erosional CLTZ (0.21°) and then up to 38 % to
635 depositional CML (0.13°). Such low slopes but high rates of change have been demonstrated
636 to be a major control on thickness variations of turbiditic beds, and behavior of turbidity
637 currents in the Moroccan turbidite system (Sumner et al., 2012) and Ogooue Fan (Mignard et
638 al., 2019). The correlation between changes in slope and erosion or deposition of eastern
639 older lobes is less obvious since longitudinal slopes evolve more gradually without major
640 slope breaks (Figs. 6a, 13).
641 Along the neochannel, the backstepping knick-point and retrogressive erosion suggest that
642 turbidity currents were much sandier than along the eastern channels. According to the
643 conceptual model in Wynn et al. (2002a), this should have promoted low efficiency flows and
644 a CLTZ smaller than to the east but this not the case. Therefore, the extra sand eroded from
645 the neochannel did not significantly modified flow efficiency or change in efficiency was

largely outpaced by another parameter such as the upper slope and slope break that are much higher than to the east.

Recent shield scaled flume tank experiments made a breakthrough in the comprehension of channel-mouth turbiditic processes, showing that lobe detachment and scouring are related to separate processes (Pohl et al., 2019; Pohl et al., 2020). The occurrence of scours is not necessary only related to slope break and hydraulic jump but more to the loss of confinement and subsequent flow relaxation (Pohl et al., 2019). On the other hand, the occurrence and size of the bypass-dominated area and the thickness of detached depositional area are controlled by the steepness of upper and lower slopes of the slope break rather than by the angle of the slope break (Pohl et al., 2020).The morphological expression of CLTZs is therefore a subtle combination of these controls, keeping in mind that a hydraulic jump will still promote erosion at a slope break. On the neofan, the large scoured area, possibly bypass-dominated, is consistent with the steep upper slope (0.26°) as shown by flume experiment (Pohl et al., 2019) while on eastern channels, smaller of absent scoured-bypass areas are consistent with the gentle upper slope (0.11-0.15°) (Figs. 6a, 13). As the expression and extension of scouring may be controlled by degree of detachment of lobes, it is therefore also indirectly controlled by the steepness of the upper slope. The degree of scouring may be related to the abruptness of the loss of confinement and flow relaxation (Pohl et al., 2020) but this is a parameter that we cannot measure. However the much bigger scours found on the neofan may be a direct consequence of bigger hydraulic jump related to the channel mouth bigger slope break.

5.6. Erosion in CLTZ: a key parameter for channels and meanders inception

Channels disconnected from the main channel, also called “headless” are common features and occur at shallow and deep-water, in small and big sedimentary systems like on pro-deltas (Gales et al., 2019), in fjords (Heijnen et al., 2020), in lakes (Girardclos et al., 2012) and on deep, basin wide, turbidite systems (Fierens et al., 2019). Here we discuss their

673 inception together with the related topic of channel sinuosity that are thoroughly addressed in
674 scientific publications (Peakall et al., 2000). Channel development is commonly described as
675 a gradual process dominantly driven by levee development and subsequent erosion
676 (Sylvester et al., 2011) but also to some extent by erosion in the channel (Babonneau et al.,
677 2002). Yet, their inception from a flat seafloor is poorly known and rarely addressed. If
678 gradual confinement of turbidity current by levee aggradation is commonly admitted, it has
679 also been outlined that seafloor erosion may play a crucial role in initial flow confinement,
680 subsequent spillover processes and eventually channel inceptions (Normark et al., 2005;
681 Fildani et al., 2006; Lastras et al., 2011; Fildani et al., 2013; Covault et al., 2014; de Leeuw et
682 al., 2016; Hodgson et al., 2016; Gales et al., 2019). Scours of various sizes and shapes are
683 well known on channel floors, overbank areas and CLTZs of many turbidite systems (e.g.
684 Palanques et al., 1995; Elliott, 2000; Kenyon et al., 2002; Wynn and Stow, 2002; Fildani and
685 Normark, 2004; Klaucke et al., 2004; Masson et al., 2004; Fildani et al., 2006; Macdonald et
686 al., 2011; Maier et al., 2011; Fildani et al., 2013; Shaw et al., 2013). In the neofan CLTZ, 15
687 km long and 10 m deep channel-like features detached from the outlet of the feeding channel
688 (Figs. 15, 16) are built by longitudinally concatenated megaflute scours (Fig. 16) indicative of
689 turbulent erosive flows (Kenyon et al., 1995; Wynn et al., 2002a; Peakall et al., 2020) on this
690 very low gradient seafloor (0.21°) at the termination of the neochannel. In addition to a
691 longitudinal concatenation, the lateral offset and shingled disposition of megaflutes mimics
692 an incipient sinuosity (Fig. 19A, B). This leads us to envisage that these megaflutes may not
693 only play a major role in channels inception but may also control, at a very early stage, a
694 sinuous pattern that is commonly interpreted as a mature stage channel-levee pattern
695 (Babonneau et al., 2002). We therefore propose that the megaflutes represent the
696 elementary structures that serve as guides to develop preferential pathways for repeated
697 erosive flows. By their constricting effects on unchannelized flows, they will eventually
698 progressively connect and evolve into immature sinuous channel-like features. The
699 confinement of turbidity current in such sinuous erosional channels (Fig. 19 B4-5) may
700 eventually develop external levees through flow striping and overspill processes and evolve

into channel-levee systems, (as observed for channel 2a1 for example, Fig. 12). This gradual development of channel will result in the gradual confinement of turbidity currents, decrease of flow relaxation and hydraulic jump and, eventually, forestepping of the CLTZ and burying of the abandoned scour marks and channel-like features under the newly developed levees, as proposed in the conceptual model of Hofstra et al. (2015).

We also assume that this process may eventually lead to the connection of the channel mouth with one of the scour-controlled channel which will virtually achieve an instantaneous progradation of the channel and channel mouth over several kilometers (Fig. 19B4-5). This hypothesis explains that the two observed scour-fields with scours of different orientations can be related to instantaneous channel mouths downslope migration (Fig. 19 C), illustrating that the channel mouths and CLTZ are dynamic area as shown in Brooks et al. (2018). This prograding process could also explain why CLTZ is not clearly observed at the outlet of channels 2 to 1.

It is noteworthy that scouring by currents of several kinds (contour currents, turbidity currents) and concatenation of scours into scour fields seem to be a major driver of channel and canyon inception in several environments. It is for instance invoked for the inception and bottom-up development of canyons on the Argentine Continental Margin under the cross processes of scouring and scours amalgamation by along-slope bottom currents and further containment and draining of across-slope turbidity currents (Lastras et al., 2011). It is also invoked for the inception of a channel avulsion on the Monterey Fan (Shepard Meander in Fildani et al., 2006; Fildani et al., 2013). Our case study has similarities with the channel inception on the Shepard Meander because it involves scouring by turbidity currents undergoing a hydraulic jump. It is however different because on the neofan, concatenation of scours occurs in the CLTZ, on a much flatter seafloor, and is, in addition, a driver for the development of channel sinuosity and for instantaneous channel progradation.

6. CONCLUSIONS

The morphology and the depositional architecture of channel mouth lobes of the Rhône fan, key architectural elements of turbitite systems, have been documented at high resolution for the first time via fine processing of DTMs, which appears as a helpful technique to highlight small topographic variations that are highly relevant to the identification and interpretation of depositional units in those environments. The opportunity to examine 8 channel avulsions and ensuing development of channel-levee, CLTZ and CML on a given mud-sand rich fan, the Rhône fan, have allowed to assume potential minimum external forcing from sea level and sediment flux changes and discuss the role of internal factors on the expression and development of channel avulsions, channel-levees systems, CLTZs and CMLs and to draw the following conclusions:

- Channel mouth lobes of the distal Late Quaternary Petit-Rhône deep-sea fan appear as elongated finger-like or pear-shaped bulges at the terminal part of a tree-like network of channel-levee systems. Their shapes and internal structure show that their emplacement is controlled by the topography and by compensational processes.
- Two main sets of channel-levee systems constitute the Late Quaternary turbidite system. The youngest, the neofan (21.5 to 18.3 cal. ka B.P.), was deposited upfan, at lower depths (2000-2500 m) with higher slope gradients (0.26°) and the neochannel was not at an equilibrium state when it was abandoned. The older channels to the east, running on the most distal parts of the fan (2500 to 2800 m water depth) on lower gradient (0.13°) appear to be at equilibrium.
- Straighter channel-levee and bad development of external levees along channels of the CML on the neofan are indicative of a lower maturity than eastern channel-levees and CMLs
- Channel-mouth lobes display noticeable morphosedimentary similarities independently of their age. The neofan shows three main domains succeeding from upstream to downstream: (1) the channel-levee system domain dominated by aggradation and channelization; (2) the Channel-Lobe Transition Zone (CLTZ)

domain *sensu stricto* with scours and channel-like features indicative of the prevalence of erosional or bypass-dominating processes; and (3) a transparent lobes domain with deposition and possibly channelization.

- On the neofan an important extension of the scoured CLTZ and detachment of the CML to the channel-levee is promoted by a high upslope before the slope break preceding the CLTZ, while for the eastern channels a low upslope before the slope break promote attachment (or less detachment) of the CML to the channel-levee. This is consistent with results from flume tank experiments (Pohl et al., 2019; Pohl et al., 2020);
- Erosion at the channel mouth and CLTZ was revealed as a major control in the inception of channel by the concatenation of scours into megaflutes, but also a major driver of incipient sinuosity at a very early stage of channel development by the shingled disposition of concatenated scours.

AKNOWLEDGEMENTS

PROGRES cruise was a contribution to the EUROSTRATAFORM European Program, (contract n° EVK3-2001-00200) and to the French Program Action Marges. This work was later realized in the framework of the Labex Mer (axis 4: Sediment transfer from coast to abyss). GRC Geociències Marines was funded by the Catalan Government (grant 2017 SGR 315) within its program for excellence research groups. Intergovernmental Oceanographic Commission (IOC) of UNESCO funded the TTR14 cruise. I. Jégou was financed by Shell during her PhD and H. Gillet benefited from a post-doctoral fellowship funded by Total. We thank the Captain, crews and onboard scientists of the R/Vs Le Suroit of Ifremer and Professor Logachef operated by the Polar Marine Geosurvey Expedition (PMGE, St. Petersburg, Russia) onboard which PROGRES (2003) and TTR14 (2004) cruises were conducted, respectively. We acknowledge the technical team from Genavir for data acquisitions during PROGRES cruise. Onboard data processing was performed by E. Le

783 Drezen and A. Normand from Ifremer and M. Rabineau, J. Baztan, G. Jouet and E. Leroux
784 from UMR6538. P. Ferrer performed part of the shore-based processing of SBP data during
785 his Master 2 research work. We acknowledge D. Aslanian (Ifremer) for permission to use and
786 publish some data acquired during the SARDINIA cruise and J.-M. Augustin (Ifremer) who
787 provided training and help for the processing of the PROGRES DTM under the SonarScope
788 software. We are grateful to Pr. D. M. Hodgson and Pr. P. J. Talling for their constructive
789 reviews, which significantly contributed to improve the manuscript.

790 **FIGURE CAPTIONS**

791 Figure 1: Location of the studied area in the framework of the Gulf of Lion, Catalan Margin
792 and Balearic Basin, modified from Droz et al. (2006). (a): Physiographic map showing the
793 turbidite systems (light grey) originating from the northern margin of the Western
794 Mediterranean and mass-transport deposits (dark grey) on the Petit-Rhône fan. (b): Shaded
795 bathymetric map of the Petit-Rhône fan basinal part. The squared areas indicate the location
796 of maps in figures 8a and 10. N is the youngest channel (neochannel); 1 is the channel that
797 was active just before N. Blue lines: location of the MAK-1M survey.

798

799 Figure 2: Method to reveal faint topographic variations at the termination of the Petit-Rhône
800 Fan, using SonarScope software. (a): Original 100 m grid PROGRES DTM. (b): Polynomial
801 surface calculated by the software that represent the first order trend (slope) of the
802 bathymetry). (c): Resulting corrected relief map obtained by subtracting (b) from (a). (d): Sun-
803 shaded relief map.

804

805 Figure 3: Main elements of the Quaternary Rhône fan channel network. (a): Successive
806 major avulsions divide the network into several branches called, from upstream to
807 downstream: the Rhône Valley connected upstream to the Petit-Rhône Canyon, the
808 Abandoned Main Channel and the principal channels (7 to 1 and neochannel, N). Grey
809 dashed lines are the limits of mass transport deposits (MTD) on both sides of the fan,
810 respectively Western Mass Transport Deposit (WMTD) and Eastern Mass Transport Deposit
811 (EMTD). (b) Groups of channels (grey, speculative boundaries). Successive minor avulsions
812 of each principal channel generate distributives channels. Channels N, 1 and 5 do not show
813 minor avulsions and constitute mono-channel groups. (c): Schematic cross sections
814 illustrating the sedimentary architecture along five transects (location in a and b).

815

816 Figure 4: Topography of the Petit-Rhône Fan South of the neochannel avulsion nodes
817 (n°15). (a): Sun-shaded bathymetric map (PROGRES 100 m-grid DTM). Eight groups of

channels (bold lettering 7 to 1 and N from the oldest to the youngest) made of 1 to 4 successive sub-channels (d to a, from the oldest to the youngest) are identifiable. Yellow and black dots and numbering of avulsion nodes same as in (d). Modified from Gillet et al. (2006). (b): Slope map of the bifurcation area between the neochannel (N) and the Abandoned Main Channel (AMC, 1) (combined PROGRES and MARION DTM). (c): Upfan to downfan serial bathymetric profiles (see locations in a, lines A to G). Grey: salt domes. Red line: course of channel 1. (d): Relative chronology of channels established from bathymetric and seismic analysis. Yellow and black dots refer respectively to main and minor (second, third and fourth order) avulsion nodes. Bold italic numbers are avulsion node numbers. Light grey area to the left refers to channels identified on the bathymetric map (a). White area to the right refers to channels identified either on the relief map (Fig. 10) or by seismic interpretation only (Fig. 11).

Figure 5: Architectural evolution of the Rhône fan. (a): Relative chronology of deposition of channel-levee systems 7 (A) to 1 (G) to N (I), from the oldest to the youngest (see Fig. 4d for the chronology of channels). For each map, the active channel is shown as a bold colored line; the preceding channels are thinner. The avulsion nodes are indicated as numbered yellow dots (major avulsions) and black dots (minor avulsions). Black arrows: Direction of channel migrations. The (H) map represents a stop of turbiditic activity during the instability period when the WMTD and EMTD (Western and Eastern Mass Transport Deposit, respectively) were emplaced. V: Valencia valley. P: Palamos valley. S: Sète valley. PLR: Pyrénéo-Languedocian Ridge. (b): Migrations of avulsion nodes through time (relative time scale) illustrated by the evolution of the distance between major (yellow bars) and minor (black bars) and a reference point chosen as the last avulsion node (n°15). Grey area and bold italic numbers are channel groups.

Figure 6: Along-thalweg profiles of the Rhône fan channels. (a): Neochannel and older channels 2c1, 2 bn, 2b1, 2a1 and 1. See Figs. 4d for the numbering of avulsion points. Black

846 and yellow dots are the positions of avulsion nodes, the yellow ones being the “major” ones
847 (see Fig. 4d). The pink dot is the main knick-point observed on the along channel depth
848 profile of the neofan. Note that the distances of older channels-lobes were measured
849 straightly and are therefore underestimated. (b): Zoom on the neochannel, modified from
850 Jégou (2008).
851
852 Figure 7: Architecture of the channel network feeding the distal lobes. Very high-resolution
853 SBP profiles (see insets for locations). (a): Strike line across the neochannel, modified from
854 Bonnel et al. (2005). (b-c): Strike lines across channels 4b and 3 to 1, PROGRES data (Droz,
855 2003). Location of SBP lines on insets.
856
857 Figure 8: Morphology of the neofan. (a): Shaded bathymetric map. Combined 50 m-grid DTM
858 from CALMAR 1997 (Loubrieu, 1997), MARION 2000 (Berné, 2000) and PROGRES 2003
859 (Droz, 2003) cruises. See location of the figure in Fig. 1b. White lines: location of SBP
860 profiles in figures 7a and 9. Box: location of figure 14a. (b): Interpretative map of a. (c): 3D
861 bathymetric view of the neofan (observed from the southwest). Blue lines (S and D) in (b) are
862 topographic profiles shown in Fig. 14b).
863
864 Figure 9: Very high-resolution SBP seismic profiles crossing the neofan (see Fig. 8a for
865 location). PROGRES data (Droz, 2003). (a): Termination of the neochannel, showing a by-
866 pass area. (b): Area with erosional channels and small scours. (c-d): Area where wedge
867 shaped seismic units dominate (d is a zoom on a wedged shape unit). Small scours are
868 visible at the NW part of the line c.
869
870 Figure 10: Detailed morphology of the distal part of the Rhône fan. (a) Sun-shaded corrected
871 relief map (see Section 3.1 and figure 2 for the method used to produce this map). The doted
872 lines outline bulges. (b) Interpretation of a. Blue continuous lines: well identified incising
873 channels. Blue dashed lines: inferred channels. Black lines: unconnected channels. Straight

874 black lines indicate the locations of profiles shown in figures 7b, 7c, 11 and 12. Dashed-
875 dotted box is the position of the maps shown in Figs. 6a and 13.
876
877 Figure 11: Upstream to downstream architectural evolution of seismic units observed under
878 the topographic bulge associated to channel 2b. Very high-resolution SBP seismic profiles,
879 PROGRES data (Droz, 2003), see Fig. 10b for location. Note on b and d the hummocky
880 areas, with symmetrical (S) and asymmetrical (A) lows that evoke scours. Vertical and
881 horizontal scales are the same in a to d and different in zooms of a, b and d.
882
883 Figure 12: Stacking pattern of terminal area of channels 2a and 2b. (a): Very high-resolution
884 3.5 kHz profiles. SARDINIA data (Aslanian et al., 2006). See Fig. 10b for location. (b): Close
885 up of a and its interpretation.
886
887 Figure 13: Slope of channels older than the neofan and their lobate basinward extensions.
888 (a) Topographic profiles of channels 2c1, 2bn, 2b1, 2a1 and 1, indicating the position of the
889 observed scours (S) and unconnected channels (UC). (b) Location of the depth profiles
890 shown in a. Distances do not account for meanders (straight distances) and are measured
891 from the uppermost avulsion node (n°14). Bold italic numbers (12, 13 and 14) refer to
892 avulsion node numbers indicated as yellow (major avulsion) and black (minor avulsion) dots
893 (see Fig. 4d for the complete numbering of avulsion nodes and Fig. 10a for the location of
894 the map).
895
896 Figure 14: Erosional features observed at the channel terminations. (a) Close up of the
897 bathymetric map of the neochannel mouth (location in Fig. 8a). (b) Topographic profiles
898 (strike line, S and dip line, D, location in a and in Fig. 8d) across the small-scours field. S:
899 symmetrical scours. A: asymmetrical scours. (c): Zoom of the relief map showing hummocky
900 areas at the terminal parts of channels 1 and 2 (location in Fig. 10) and location dip profiles
901 shown in d. (d): Dip topographic profiles (D1 and D2), showing mainly asymmetrical

902 topographic features, similar to that of the neofan, even if smaller (compare with b, same
903 vertical and horizontal scales).
904
905 Figure 15: Shaded bathymetry of the neofan area (illumination from the East). Compilation of
906 DTM from MARION (Berné, 2000) and PROGRES (Droz, 2003) cruises at a grid spacing of
907 50 m. (a): Bathymetry of the neochannel and its termination. (b) Close up of channel-like
908 features associated to semi-circular scarps some km from the termination of the neochannel;
909 Ch1 to Ch4 are numbered without age inference. (c) Close up of chevron-like features in the
910 distal part of the neofan.
911
912 Figure 16: Detailed topography of channel-like Ch2 downwards its bifurcation from Ch1. (a):
913 MAK-1M mosaic and its interpretation. See location in figure 15b. (b) and (c): MAK-1M
914 profiles (not corrected for navigation) and associated 5 kHz profile at the head (b) and the
915 distal part (c) of Ch2 (location in a). S1 to S4 refer to scour numbers (no chronological
916 inference).
917
918 Figure 17: Morpho-structural interpretative maps. (a): Synthesis of studied channel-levee
919 systems replaced in the context of the Late Quaternary depositional systems of the Gulf of
920 Lion (see Fig. 1a for legends about depositional systems other than the Petit-Rhône turbidite
921 system) showing the proposed extension of the 3 main morpho-structural domains. Bold
922 numbers refer to groups of channels. Arrows indicate the directions of lateral migration
923 consecutive to avulsions for different hierarchical orders. (b): Chronology of seismic bodies
924 identified in the distal parts of the Rhône fan, established from overlapping relationships
925 observed on SBP profiles. (c): Main dimensions measured and reported in Tables 1 and 2.
926 Lengths are measured straightly and therefore are underestimated. TL and TW: total length
927 (measured from the Petit-Rhône canyon head) and maximum total width of the fan,
928 respectively; L1, L2 and L3: length of domains 1 (measured from the avulsion node from

929 which the channels are issued), 2 and 3, respectively; W1, W2 and W3: maximum width of
930 domains 1, 2 and 3, respectively.
931
932 Figure 18: Morphometric analysis of domains 3 of the morphological bulges 2bn, 2b1, 2a1, 1
933 and N. (a): Log-Log plot of the maximum width to maximum thickness. (b): Log-Log plot of
934 the length/width (aspect ratio) to maximum thickness/maximum area. Inspired from Prélat et
935 al. (2010). See Supplementary Material for details of measurements. Due to incomplete
936 coverage, maximum width and maximum area for domain 3 of bulge 1 are minimum.
937
938 Figure 19: Proposed formation of sinuous channel-levee systems on a very low gradient
939 seafloor, ultimately leading to basinwards propagation of the channel. (A) Conceptual
940 evolution of the scours field during progressive flow containment. (B) Application to the
941 Rhône neofan.(1 to 3): scour controlled initiation of a sinuous channel (based on
942 observations in the neofan, see Figs. 15, 16). (4 and 5): hypothesized further evolution
943 towards a sinuous channel-levee system (4) that could prograde basinwards by connection
944 with the previous neochannel mouth (5). The box inside (5) locates sketches 1 to 4. (C)
945 Evolution through time of the neochannel mouth (CM 1 and CM 2) and associated scour
946 fields (CLTZ 1 and CLTZ 2), showing a possible next CM (if the neofan was not abandoned
947 after CM2).
948
949 **TABLE CAPTIONS**

950 Table 1: Architecture and known ages of the Rhône fan and CMLs (neofan and older CMLs
951 2c to 1). See Fig. 17b for explanations of measured dimensions TW and TL, D14 and D15.
952
953 Table 2: Sizes of the Rhône CMLs (systems 2c to 1 and neofan) and of the erosional
954 features (scours and unconnected channels) and wedge-shaped seismic units. See Fig. 17b
955 for explanations of measured dimensions W and L.

REFERENCES

Amy, L. A., 2019. A review of producing fields inferred to have upslope stratigraphically trapped turbidite reservoirs: Trapping styles (pure and combined), pinch-out formation, and depositional setting. Aapg Bulletin, 103 (12): 2861-2889. DOI: 10.1306/02251917408.

Aslanian, D., Geli, L. and Olivet, J. L., 2006. SARDINIA cruise, RV L'Atalante. DOI: 10.17600/6010150.

Babonneau, N., Savoye, B., Cremer, M. and Klein, B., 2002. Morphology and architecture of the present canyon and channel system of the Zaire deep-sea fan. Marine and Petroleum Geology, 19 (4): 445-467. DOI: 10.1016/S0264-8172(02)00009-0.

Badhani, S., Cattaneo, A., Dennielou, B., Leroux, E., Colin, F., Thomas, Y., Jouet, G., Rabineau, M. and Droz, L., 2020. Morphology of retrogressive failures in the Eastern Rhone Interfluve during the Last Glacial Maximum (Gulf of Lions, Western Mediterranean). Geomorphology, 351: 106894. DOI: 10.1016/j.geomorph.2019.106894.

Bassetti, M. A., Berne, S., Jouet, G., Taviani, M., Dennielou, B., Flores, J. A., Gaillot, A., Gelfort, R., Lafuerza, S. and Sultan, N., 2008. The 100-ka and rapid sea level changes recorded by prograding shelf sand bodies in the Gulf of Lions (western Mediterranean Sea). Geochemistry Geophysics Geosystems, 9. DOI: 10.1029/2007gc001854.

Bassetti, M. A., Jouet, G., Dufois, F., Berne, S., Rabineau, M. and Taviani, M., 2006. Sand bodies at the shelf edge in the Gulf of Lions (Western Mediterranean): Deglacial history and modern processes. Marine Geology, 234 (1-4): 93-109. DOI: 10.1016/j.margeo.2006.09.010.

Baztan, J., Berne, S., Olivet, J. L., Rabineau, M., Aslanian, D., Gaudin, A., Rehault, J. P. and Canals, M., 2005. Axial incision: The key to understand submarine canyon evolution (in the western Gulf of Lion). Marine and Petroleum Geology, 22 (6-7): 805-826. DOI: 10.1016/j.marpetgeo.2005.03.011.

Bellaiche, G., Coutellier, V. and Droz, L., 1986. Seismic evidence of widespread mass transport deposits in the Rhône deep-sea fan: Their role in the fan construction. Marine Geology, 89: 259-268. DOI: 10.1016/0025-3227(86)90076-9.

983 Berné, S., 2000. MARION cruise, RV Le Suroît. DOI: 10.17600/20110.
984 Berné, S., Aloïsi, J. C., Baztan, J., Dennielou, B., Droz, L., dos Reis, A. T., Lofi, J., Méar, Y.
985 and Rabineau, M., 2002a. Notice de la carte morpho-bathymétrique du Golfe du Lion. 48 pp.
986 Berné, S., Carré, D., Loubrieu, B., Mazé, J.-P. and Normand, A., 2001. Carte morpho-
987 bathymétrique du Golfe du Lion à l'échelle 1/100 000 ème. Brest, IFREMER et Région
988 Languedoc Roussillon.
989 Berné, S., Satra, C., Aloïsi, J. C., Baztan, J., Dennielou, B., Droz, L., Dos Reis, A. T., Lofi, J.,
990 Méar, Y. and Rabineau, M., 2002b. Carte morpho-bathymétrique du Golfe du Lion, notice
991 explicative. Ifremer, Brest.
992 Bonnel, C., Dennielou, B., Droz, L., Mulder, T. and Berné, S., 2005. Architecture and
993 depositional pattern of the Rhône Neofan and recent gravity activity in the Gulf of Lions
994 (Western Mediterranean). Marine and Petroleum Geology, 22 (6-7): 827-843. DOI:
995 10.1016/j.marpetgeo.2005.03.003.
996 Brooks, H. L., Hodgson, D. M., Brunt, R. L., Peakall, J., Hofstra, M. and Flint, S. S., 2018.
997 Deep-water channel-lobe transition zone dynamics: Processes and depositional architecture,
998 an example from the Karoo Basin, South Africa. Geological Society of America Bulletin, 130
999 (9-10): 1723-1746. DOI: 10.1130/b31714.1.
1000 Canals, M., Puig, P., Durrieu de Madron, X., Heussner, S., Palanques, A. and Fabres, J.,
1001 2006. Flushing submarine canyons. Nature, 444 (7117): 354-355. DOI:
1002 10.1038/nature05271.
1003 Carvajal, C., Paull, C. K., Caress, D. W., Fildani, A., Lundsten, E., Anderson, K., Maier, K. L.,
1004 McGann, M., Gwiazda, R. and Herguera, J. C., 2017. Unraveling the channel-lobe Transition
1005 zone with high-resolution AUV bathymetry: Navy Fan, offshore Baja California, Mexico
1006 Journal of Sedimentary Research, 87 (10): 1049-1059. DOI: 10.2110/jsr.2017.58.
1007 Covault, J. A., Kostic, S., Paull, C. K., Ryan, H. F. and Fildani, A., 2014. Submarine channel
1008 initiation, filling and maintenance from sea-floor geomorphology and morphodynamic
1009 modelling of cyclic steps. Sedimentology, 61 (4): 1031-1054. DOI: 10.1111/sed.12084.

de Leeuw, J., Eggenhuisen, J. T. and Cartigny, M. J. B., 2016. Morphodynamics of submarine channel inception revealed by new experimental approach. Nature Communications, 7:10886. DOI: 10.1038/ncomms10886.

Dennielou, B., Droz, L., Babonneau, N., Jacq, C., Bonnel, C., Picot, M., Le Saout, M., Saout, Y., Bez, M., Savoye, B., Olu, K. and Rabouille, C., 2017. Morphology, structure, composition and build-up processes of the active channel-mouth lobe complex of the Congo deep-sea fan with inputs from remotely operated underwater vehicle (ROV) multibeam and video surveys. Deep-Sea Research Part II-Topical Studies in Oceanography, 142: 25-49. DOI: 10.1016/j.dsr2.2017.03.010.

Dennielou, B., Jallet, L., Sultan, N., Jouet, G., Giresse, P., Voisset, M. and Berné, S., 2009. Post-glacial persistence of turbiditic activity within the Rhone deep-sea turbidite system (Gulf of Lions, Western Mediterranean): Linking the outer shelf and the basin sedimentary records. Marine Geology, 257 (1-4): 65-86. DOI: 10.1016/j.margeo.2008.10.013.

Dennielou, B., Jegou, I., Droz, L., Jouet, G., Cattaneo, A., Aslanian, D., Berné, S., Loubrieu, B., Rabineau, M., Sultan, N. and Bermell, S., 2019. Major modification of sediment routing by a giant Mass Transport Deposit in the Gulf of Lions (Western Mediterranean). Marine Geology, 411: 1-20. DOI: 10.1016/j.margeo.2019.01.011.

Deptuck, M. E., Piper, D. J. W., Savoye, B. and Gervais, A., 2008. Dimensions and architecture of late Pleistocene submarine lobes off the northern margin of East Corsica. Sedimentology, 55 (4): 869-898. DOI: 10.1111/j.1365-3091.2007.00926.x.

Deptuck, M. E., Steffens, G. S., Barton, M. and Pirmez, C., 2003. Architecture and evolution of upper fan channel-belts on the Niger Delta slope and in the Arabian Sea. Marine And Petroleum Geology, 20 (6-8): 649-676.

Dorrell, R. M., Peakall, J., Sumner, E. J., Parsons, D. R., Darby, S. E., Wynn, R. B., Özsoy, E. and Tezcan, D., 2016. Flow dynamics and mixing processes in hydraulic jump arrays: Implications for channel-lobe transition zones. Marine Geology, 381: 181-193. DOI: 10.1016/j.margeo.2016.09.009.

dos Reis, A. T., 2001. La tectonique salifère et son influence sur l'architecture sédimentaire quaternaire de la marge du Golfe du Lion, Méditerranée Occidentale - 2 Volumes. PhD Thesis, Paris 6 University. 373 pp.

dos Reis, A. T., Gorini, C. and Mauffret, A., 2005. Implications of salt-sediment interactions on the architecture of the Gulf of Lions deep-water sedimentary systems-western Mediterranean Sea. Marine and Petroleum Geology, 22 (6-7): 713-746. DOI: 10.1016/j.marpetgeo.2005.03.006.

Droz, L., 2003. PROGRES cruise, RV Le Suroît. DOI: 10.17600/3020080.

Droz, L. and Bellaiche, G., 1985. Rhone Deep-Sea Fan: morphostructure and growth pattern. American Association of Petroleum Geologists Bulletin, 69: 460-479.

Droz, L., dos Reis, A. T., Rabineau, M., Berné, S. and Bellaiche, G., 2006. Quaternary turbidite systems on the northern margins of the Balearic Basin (Western Mediterranean): a synthesis. Geo-Marine Letters, 26 (6): 347-359. DOI: 10.1007/s00367-006-0044-0.

Droz, L., Kergoat, R., Cochonat, P. and Berné, S., 2001. Recent sedimentary events in the western Gulf of Lions (Western Mediterranean). Marine Geology, 176 (1-4): 23-37. DOI: 10.1016/s0025-3227(01)00147-5.

Droz, L., Marsset, T., Ondreas, H., Lopez, M., Savoye, B. and Spy-Anderson, F. L., 2003a. Architecture of an active mud-rich turbidite system: The Zaire Fan (Congo-Angola margin southeast Atlantic): Results from ZaiAngo 1 and 2 cruises. AAPG Bulletin, 87 (7): 1145-1168. DOI: 10.1306/03070300013.

Droz, L., Rabineau, M. and Progres Shipboard Scientific Party, 2003b. Interrelationships between the sedimentary systems in the Western Mediterranean (Gulf of Lions and Balearic Abyssal Plain): preliminary results from PROGRES cruise (EUROSTRATAFORM programme). Ocean Margin Research Conference, OMARC, Paris.

Elliott, T., 2000. Megaflute erosion surfaces and the initiation of turbidite channels. Geology, 28 (2): 119-122. DOI: 10.1130/0091-7613(2000)28<119:MESATI>2.0.CO;2.

Fierens, R., Droz, L., Toucanne, S., Raisson, F., Jouet, G., Babonneau, N., Miramontes, E., Landurain, S. and Jorry, S. J., 2019. Late Quaternary geomorphology and sedimentary

1065 processes in the Zambezi turbidite system (Mozambique Channel). Geomorphology, 334: 1-
1066 28. DOI: 10.1016/j.geomorph.2019.02.033.
1067 Fildani, A., Hubbard, S. M., Covault, J. A., Maier, K. L., Romans, B. W., Traer, M. and
1068 Rowland, J. C., 2013. Erosion at inception of deep-sea channels. Marine and Petroleum
1069 Geology, 41: 48-61. DOI: 10.1016/j.marpetgeo.2012.03.006.
1070 Fildani, A. and Normark, W. R., 2004. Late Quaternary evolution of channel and lobe
1071 complexes of Monterey Fan. Marine Geology, 206 (1-4): 199-223. DOI:
1072 10.1016/j.margeo.2004.03.001.
1073 Fildani, A., Normark, W. R., Kostic, S. and Parker, G., 2006. Channel formation by flow
1074 stripping: large-scale scour features along the Monterey East Channel and their relation to
1075 sediment waves. Sedimentology, 53: 1265-1287. DOI: 10.1111/j.1365-3091.2006.00812.x.
1076 Flood, R. C., Manley, P. L., Kowsmann, K. O., Appi, C. J. and Pirmez, C., 1991. Seismic
1077 facies and late Quaternary growth of Amazon submarine fan. Seismic Facies and
1078 Sedimentary Processes of Submarine Fans and Turbidite Systems. P. Weimer and M. H.
1079 Link. NewYork, Springer-Verlag**:** 415-434.
1080 Gales, J. A., Talling, P. J., Cartigny, M. J. B., Clarke, J. H., Lintern, G., Stacey, C. and Clare,
1081 M. A., 2019. What controls submarine channel development and the morphology of deltas
1082 entering deep-water fjords? Earth Surface Processes and Landforms, 44 (2): 535-551. DOI:
1083 10.1002/esp.4515.
1084 Gaudin, M., Berné, S., Jouanneau, J.-M., Palanques, A., Puig, P., Mulder, T., Cirac, P.,
1085 Rabineau, M. and Imbert, P., 2006. Massive sand beds attributed to deposition by dense
1086 water cascades in the Bourcart canyon head, Gulf of Lions (northwestern Mediterranean
1087 Sea). Marine Geology, 234 (1-4): 111-128. DOI: 10.1016/j.margeo.2006.09.020.
1088 Gaullier, V., Antonini, E., Benkhelil, J. and Got, H., 1998. Recent gravity-driven sedimentary
1089 bodies in the North-Balearic Basin: geometry and quantification. Comptes Rendus de
1090 l'Académie des Sciences - Series IIA - Earth and Planetary Science, 327 (10): 677-684. DOI:
1091 10.1016/S1251-8050(99)80025-1.

1092 Gillet, H., Droz, L., Savoye, B. and Bez, M., 2006. Morphostructure of the channel/levee
1093 complexes and correlative terminal lobes of the Petit-Rhône Fan (Western Mediterranean):
1094 Results from PROGRES cruise (EUROSTRATAFORM Project). European Geosciences
1095 Union General Assembly, Vienna, Austria, 2-7 April 2006.
1096 Girardclos, S., Hilbe, M., Corella, J. P., Loizeau, J.-L., Kremer, K., DelSontro, T., Arantegui,
1097 A., Moscariello, A., Arlaud, F., Akhtman, Y., Anselmetti, F. S. and Lemmin, U., 2012.
1098 Searching the Rhone delta channel in Lake Geneva since François-Alphonse Forel. Archive
1099 des Sciences, 65 (1-2): 103-118.
1100 Guiastrennec-Faugas, L., Gillet, H., Jacinto, R. S., Dennielou, B., Hanquiez, V., Schmidt, S.,
1101 Simplet, L. and Rousset, A., 2020. Upstream migrating knickpoints and related sedimentary
1102 processes in a submarine canyon from a rare 20-year morphobathymetric time-lapse
1103 (Capbreton submarine canyon, Bay of Biscay, France). Marine Geology, 423: 6143-6143.
1104 Heijnen, M. S., Clare, M. A., Cartigny, M. J. B., Talling, P. J., Hage, S., Lintern, D. G.,
1105 Stacey, C., Parsons, D. R., Simmons, S. M., Chen, Y., Sumner, E. J., Dix, J. K. and Hughes
1106 Clarke, J. E., 2020. Rapidly-migrating and internally-generated knickpoints can control
1107 submarine channel evolution. Nature Communications, 11 (1): 3129. DOI: 10.1038/s41467-
1108 020-16861-x.
1109 Hodgson, D. M., Kane, I. A., Flint, S. S., Brunt, R. L. and Ortiz-Karpf, A., 2016. Time-
1110 transgessive confinement on the slope and the progradation of basin-floor fans: implications
1111 for the sequence stratigraphy of deep-water deposits. Journal of Sedimentary Research, 86
1112 (2): 73-86. DOI: 10.2110/jsr.2016.3.
1113 Hofstra, M., Hodgson, D. M., Peakall, J. and Flint, S. S., 2015. Giant scour-fills in ancient
1114 channel-lobe transition zones: Formative processes and depositional architecture.
1115 Sedimentary Geology, 329: 98-114. DOI: 10.1016/j.sedgeo.2015.09.004.
1116 Jallet, L. and Giresse, P., 2005. Construction of the Pyreneo-Languedocian Sedimentary
1117 Ridge and associated sediment waves in the deep western Gulf of Lions (Western
1118 Mediterranean). Marine and Petroleum Geology, 22 (6-7): 865-888. DOI:
1119 10.1016/j.marpetgeo.2005.03.008.

1120 Jégou, I., 2008. Etude de la transition chenal-levées lobes dans les systèmes turbiditiques
1121 récents. Application à l'éventail turbiditique de l'Amazone et au Néofan du Petit-Rhône. PhD
1122 Thesis, Brest University (UBO). 350 pp.
1123 Jégou, I., Savoye, B., Pirmez, C. and Droz, L., 2008. Channel-mouth lobe complex of the
1124 recent Amazon Fan: The missing piece. Marine Geology, 252: 62-77. DOI:
1125 10.1016/j.margeo.2008.03.004.
1126 Kane, I. A., McCaffrey, W. D. and Martinsen, O. J., 2009. Allogenic vs. autogenic controlson
1127 Megaflute Formation. Journal of Sedimentary Research, 79 (9-10): 643-651. DOI:
1128 10.2110/jsr.2009.072.
1129 Kenyon, N., Ivanov, M. K., Akhmetzhanov, A. M. and Kozlova, E. V., 2006. Interdisciplinary
1130 geoscience studies of the Gulf of Cadiz and Western Mediterranean basins. Preliminary
1131 results of investigations during the TTR-14 cruise of RV Professor Logachev July-
1132 September, 2004. United Nations Educational, Scientific and Cultural Organisation
1133 (UNESCO). Intergovernmental Oceanographic Commission.
1134 Kenyon, N. H., Klaucke, I., Millington, J. and Ivanov, M. K., 2002. Sandy submarine canyon-
1135 mouth lobes on the western margin of Corsica and Sardinia, Mediterranean Sea. Marine
1136 Geology, 184 (1-2): 69-84. DOI: 10.1016/S0025-3227(01)00282-1.
1137 Kenyon, N. H., Millington, J., Droz, L. and Ivanov, M. K., 1995. Scour holes in a channel-lobe
1138 transition zone on the Rhône cone. Atlas of Deep-Water Environments: Architectural Styles
1139 in Turbidite Systems. K. T. Pickering, R. N. Hiscott, N. H. Kenyon, F. R. Lucchi and R. D. A.
1140 Smith. London, Chapman and Hall**:** 212-215.
1141 Klaucke, I., Masson, D. G., Kenyon, N. H. and Gardner, J. V., 2004. Sedimentary processes
1142 of the lower Monterey Fan channel and channel-mouth lobe. Marine Geology, 206 (1-4): 181-
1143 198. DOI: 10.1016/j.margeo.2004.02.006.
1144 Kolla, V., 2007. A review of sinuous channel avulsion patterns in some major deep-sea fans
1145 and factors controlling them. Marine and Petroleum Geology, 24 (6-9): 450-469.
1146 Komar, P. D., 1971. Hydraulic jumps in turbidity currents. Geological Society of America
1147 Bulletin, 82: 1477-1488.

1148 Labeyrie, L., Jansen, E. and Cortijo, E., 2003. MD 114-Images V à bord du Marion Dufresne.
1149 Institut polaire français Paul-Emile Victor. ISBN: 978-2-910180-29-4.
1150 Lastras, G., Acosta, J., Munoz, A. and Canals, M., 2011. Submarine canyon formation and
1151 evolution in the Argentine Continental Margin between 44 degrees 30 ' S and 48 degrees S.
1152 Geomorphology, 128 (3-4): 116-136. DOI: 10.1016/j.geomorph.2010.12.027.
1153 Lastras, G., Canals, M., Amblas, D., Ivanov, M., Dennielou, B., Droz, L. and Akhmetzhanov,
1154 A., 2006. Eivissa slides, western Mediterranean Sea: morphology and processes. Geo-
1155 Marine Letters, 26 (4): 225-233. DOI: 10.1007/s00367-006-0032-4.
1156 Lastras, G., Canals, M., Urgeles, R., De Batist, M., Calafat, A. M. and Casamor, J. L., 2004.
1157 Characterisation of the recent BIG'95 debris flow deposit on the Ebro margin, Western
1158 Mediterranean Sea, after a variety of seismic reflection data. Marine Geology, 213 (1-4): 235-
1159 255. DOI: 10.1016/j.margeo.2004.10.008.
1160 Leroux, E., 2012. Quantification des flux sédimentaires et de la subsidence du bassin
1161 provençal. PhD Thesis, Brest University. 445 pp.
1162 Leroux, E., Rabineau, M., Aslanian, D., Gorini, C., Molliex, S., Bache, F., Robin, C., Droz, L.,
1163 Moulin, M., Poort, J., Rubino, J. L. and Suc, J. P., 2017. High-resolution evolution of
1164 terrigenous sediment yields in the Provence Basin during the last 6 Ma: relation with climate
1165 and tectonics. Basin Research, 29 (3): 305-339. DOI: 10.1111/bre.12178.
1166 Leroux, E., Rabineau, M., Aslanian, D., Granjeon, D., Droz, L. and Gorini, C., 2014.
1167 Stratigraphic simulations of the shelf of the Gulf of Lions: testing subsidence rates and sea-
1168 level curves during the Pliocene and Quaternary. Terra Nova, 26 (3): 230-238. DOI:
1169 10.1111/ter.12091.
1170 Lofi, J., Rabineau, M., Gorini, C., Berne, S., Clauzon, G., De Clarens, P., Dos Reis, A. T.,
1171 Mountain, G. S., Ryan, W. B. F., Steckler, M. S. and Fouchet, C., 2003. Plio-Quaternary
1172 prograding clinoform wedges of the western Gulf of Lion continental margin (NW
1173 Mediterranean) after the Messinian Salinity Crisis. Marine Geology, 198 (3-4): 289-+. DOI:
1174 10.1016/s0025-3227(03)00120-8.

1175 Lombo-Tombo, S., Dennielou, B., Berne, S., Bassetti, M. A., Toucanne, S., Jorry, S. J.,
1176 Jouet, G. and Fontanier, C., 2015. Sea-level control on turbidite activity in the Rhone canyon
1177 and the upper fan during the Last Glacial Maximum and Early deglacial. Sedimentary
1178 Geology, 323: 148-166. DOI: 10.1016/j.sedgeo.2015.04.009.
1179 Lonsdale, P. L. and Hollister, C. D., 1979. Cut-offs at an abyssal meander south of Iceland.
1180 Geology (7): 597-601. DOI: 10.1130/0091-7613(1979)7<597:CAAAMS>2.0.CO;2.
1181 Lopez, M., 2001. Architecture and depositional pattern of the Quaternary deep-sea fan of the
1182 Amazon. Marine and Petroleum Geology, 18 (4): 479-486. DOI: 10.1016/S0264-
1183 8172(00)00071-4.
1184 Loubrieu, B., 1997. CALMAR97 cruise, RV L'Atalante.
1185 Macdonald, H. A., Wynn, R. B., Huvenne, V. A. I., Peakall, J., Masson, D. G., Weaver, P. P.
1186 E. and McPhail, S. D., 2011. New insights into the morphology, fill, and remarkable longevity
1187 (> 0.2 m.y.) of modern deep-water erosional scours along the northeast Atlantic margin.
1188 Geosphere, 7 (4): 845-867. DOI: 10.1130/GES00611.1.
1189 Maier, K. L., Fildani, A., Paull, C. K., Graham, S. A., McHargue, T. R., Caress, D. W. and
1190 McGann, M., 2011. The elusive character of discontinuous deep-water channels: New
1191 insights from Lucia Chica channel system, offshore California. Geology, 39 (4): 327-330.
1192 DOI: 10.1130/G31589.1.
1193 Maier, K. L., Paull, C. K., Caress, D. W., Anderson, K., Nieminski, N. M., Lundsten, E., Erwin,
1194 B. E., Gwiazda, R. and Fildani, A., 2020. SUBMARINE-FAN DEVELOPMENT REVEALED
1195 BY INTEGRATED HIGH-RESOLUTION DATASETS FROM LA JOLLA FAN, OFFSHORE
1196 CALIFORNIA, USA. Journal of Sedimentary Research, 90 (5): 468-479. DOI:
1197 10.2110/jsr.2020.22.
1198 Mansor, S., 2009. Avulsion process in turbidite sytems: Stratigraphic and lithologic records.
1199 Application to the Amazon and Zaire turbidite systems. PhD Thesis, Brest University (UBO).
1200 225 pp.

1201 Marsset, T. and Bellec, V., 2002. Late Pleistocene-Holocene deposits of the Rhône inner
1202 continental shelf (France): Detailed mapping and correlation with previous continental and
1203 marine studies. Sedimentology, 49: 255-276. DOI: 10.1046/j.1365-3091.2002.00440.x.
1204 Masson, D. G., Wynn, R. B. and Bett, B. J., 2004. Sedimentary environment of the Faroe-
1205 Shetland and Faroe Bank Channels, north-east Atlantic, and the use of bedforms as
1206 indicators of bottom current velocity in the deep ocean. Sedimentology, 51 (6): 1207-1241.
1207 DOI: 10.1111/j.1365-3091.2004.00668.x.
1208 Menard, H. W., Smith, S. M. and Pratt, R. M., 1965. The Rhone deep-sea Fan. Submarine
1209 Geology and Geophysics (Proceedings of the 17th Symposium of the Colstan Research
1210 Society). W. F. Whittard and R. Bradshaw. London, Buttersworth**:** 271-285.
1211 Migeon, S., Ducassou, E., Le Gonidec, Y., Rouillard, P., Mascle, J. and Revel-Rolland, M.,
1212 2010. Lobe construction and sand/mud segregation by turbidity currents and debris flows on
1213 the western Nile deep-sea fan (Eastern Mediterranean). Sedimentary Geology, 229 (3): 124-
1214 143. DOI: 10.1016/j.sedgeo.2010.02.011.
1215 Mignard, S., Mulder, T., Martinez, P. and Garlan, T., 2019. The Ogooue Fan (offshore
1216 Gabon): a modern example of deep-sea fan on a complex slope profile. Solid Earth, 10 (3):
1217 851-869. DOI: 10.5194/se-10-851-2019.
1218 Molliex, S., Rabineau, M., Leroux, E., Bourles, D. L., Authemayou, C., Aslanian, D., Chauvet,
1219 F., Civet, F. and Jouet, G., 2016. Multi-approach quantification of denudation rates in the
1220 Gulf of Lion source-to-sink system (SE France). Earth and Planetary science Letters, 444:
1221 101-115. DOI: 10.1016/j.epsl.2016.03.043.
1222 Mulder, T. and Etienne, S., 2010. Lobes in deep-sea turbidite systems: State of the art
1223 Preface. Sedimentary Geology, 229 (3): 75-80. DOI: 10.1016/j.sedgeo.2010.06.011.
1224 Mutti, E. and Normark, W. R., 1987. Comparing examples of modern and ancient turbidite
1225 systems: problems and concepts. Marine Clastic Sedimentology. L. J.K. and Z. G.G. London,
1226 Graham and Trotman**:** 1-38.

1227 Normark, W. R., Fildani, A., Kostic, S. and Parker, G., 2005. Large kilometer-scale erosional
1228 depositional bedforms as a result of turbidity-current overflow from the Monterey Channel.
1229 American Association of Petroleum Geologists Annual Convention, Calgary, Canada.
1230 O'Connell, S., McHugh, C. and Ryan, W. B. F., 1995. Unique fan morphology in an
1231 entrenched thalweg channel on the Rhône Fan. Atlas of Deep Water Environments :
1232 Architectural style in turbidite systems. K. T. Pickering, R. N. Hiscott, N. H. Kenyon, F. Ricci
1233 Luchi and R. D. A. Smith. Aberdeen, Chapman & Hall**:** 80-83.
1234 O'Connell, S., Normark, W. R., Ryan, W. B. F. and Kenyon, N. H., 1991. An entrenched
1235 thalweg channel on the Rhône fan : interpretation from a SEABEAM and SEAMARC I
1236 survey. From Shoreline to Abyss: Contributions to Marine Geology in Honor of Francis
1237 Parker Shepard. R. H. Osborne, SEPM Special Publication. 46**:** 259-270.
1238 Ortiz-Karpf, A., Hodgson, D. M. and McCaffrey, W. D., 2015. The role of mass-transport
1239 complexes in controlling channel avulsion and the subsequent sediment dispersal patterns
1240 on an active margin: The Magdalena Fan, offshore Colombia. Marine and Petroleum
1241 Geology, 64: 58-75. DOI: 10.1016/j.marpetgeo.2015.01.005.
1242 Palanques, A., de Madron, X. D., Puig, P., Fabres, J., Guillen, J., Calafat, A., Canals, M.,
1243 Heussner, S. and Bonnin, J., 2006. Suspended sediment fluxes and transport processes in
1244 the Gulf of Lions submarine canyons. The role of storms and dense water cascading. Marine
1245 Geology, 234 (1-4): 43-61. DOI: 10.1016/j.margeo.2006.09.002.
1246 Palanques, A., Kenyon, N. H., Alonso, B. and Limonov, A., 1995. Erosional and Depositional
1247 Patterns in the Valencia Channel Mouth: An Exemple of a Modern Channel-Lobe Transition
1248 Zone. Marine Geophysical Researches, 17: 503-517. DOI: 10.1007/BF01204341.
1249 Peakall, J., Best, J., Baas, J. H., Hodgson, D. M., Clare, M. A., Talling, P. J., Dorrell, R. M.
1250 and Lee, D. R., 2020. An integrated process-based model of flutes and tool marks in deep-
1251 water environments: Implications for palaeohydraulics, the Bouma sequence and hybrid
1252 event beds. Sedimentology, 67 (4): 1601-1666. DOI: 10.1111/sed.12727.

1253 Peakall, J., McCaffrey, B. and Kneller, B., 2000. A process model for the evolution,
1254 morphology, and architecture of sinuous submarine channels. Journal of Sedimentary
1255 Research, 70 (3): 434-448.
1256 Picot, M., 2015. Cycles sédimentaires dans le système turbiditique du Congo : nature et
1257 origine. PhD thesis, Brest University (UBO). 368 pp.
1258 Picot, M., Droz, L., Marsset, T., Dennielou, B. and Bez, M., 2016. Controls on turbidite
1259 sedimentation: Insights from a quantitative approach of submarine channel and lobe
1260 architecture (Late Quaternary Congo fan). Marine and Petroleum Geology, 72: 423-446. DOI:
1261 10.1016/j.marpetgeo.2016.02.004.
1262 Piper, D. J. W. and Normark, W. R., 2001. Sandy fans - from Amazon to Hueneme and
1263 beyond. American Association of Petroleum Geologist Bulletin, 85 (8): 1407-1438.
1264 Pirmez, C. and Flood, R. D., 1995. Morphology and structure of Amazon Channel.
1265 Proceedings of the Ocean Drilling Program, Initial Reports. R. D. Flood, D. J. W. Piper and A.
1266 Klaus. College Station, TX, Ocean Drilling Program. 155**:** 23-45.
1267 Pirmez, C., Hiscott, R. N. and Kronen, J. D. J., 1997. Sandy turbidite successions at the base
1268 of channel-levee systems of the Amazon fan revealed by FMS logs and cores: unravelling
1269 the facies architecture of large submarine fans. Proceedings of the Ocean Drilling Program,
1270 Scientific Results. R. D. Flood, D. J. W. Piper, A. Klaus and L. C. Peterson. Austin, Tx, ODP.
1271 155**:** 7-33.
1272 Pirmez, C. and Imran, J., 2003. Reconstruction of turbidity currents in Amazon Channel.
1273 Marine and Petroleum Geology, 20 (6-8): 823-849.
1274 Pohl, F., Eggenhuisen, J. T., Cartigny, M. J. B., Tilston, M. C., de Leeuw, J. and Hermidas,
1275 N., 2020. The influence of a slope break on turbidite deposits: An experimental investigation.
1276 Marine Geology, 424. DOI: 10.1016/j.margeo.2020.106160.
1277 Pohl, F., Eggenhuisen, J. T., Tilston, M. and Cartigny, M. J. B., 2019. New flow relaxation
1278 mechanism explains scour fields at the end of submarine channels. Nature Communications,
1279 10. DOI: 10.1038/s41467-019-12389-x.

1280 Popescu, I., Lericolais, G., Panin, N., Wong, H. K. and Droz, L., 2001. Late Quaternary
1281 channel avulsions on the Danube deep-sea fan, Black Sea. Marine Geology, 179 (1-2): 25-
1282 37.
1283 Prélat, A., Covault, J. A., Hodgson, D. M., Fildani, A. and Flint, S. S., 2010. Intrinsic controls
1284 on the range of volumes, morphologies, and dimensions of submarine lobes. Sedimentary
1285 Geology, 232 (1-2): 66. DOI: 10.1016/j.sedgeo.2010.09.010.
1286 Prélat, A., Hodgson, D. M. and Flint, S. S., 2009. Evolution, architecture and hierarchy of
1287 distributary deep-water deposits: a high-resolution outcrop investigation from the Permian
1288 Karoo Basin, South Africa. Sedimentology, 56 (7): 2132-U2125. DOI: 10.1111/j.1365-
1289 3091.2009.01073.x.
1290 Rabineau, M., Berne, S., Olivet, J.-L., Aslanian, D., Guillocheau, F. and Joseph, P., 2006.
1291 Paleo sea levels reconsidered from direct observation of paleoshoreline position during
1292 Glacial Maxima (for the last 500,000 yr). Earth and Planetary science Letters, 252 (1-2): 119-
1293 137. DOI: 10.1016/j.epsl.2006.09.033.
1294 Rabineau, M., Leroux, E., Aslanian, D., Bache, F., Gorini, C., Moulin, M., Molliex, S., Droz,
1295 L., dos Reis, A. T., Rubino, J. L., Guillocheau, F. and Olivet, J. L., 2014. Quantifying
1296 subsidence and isostatic readjustment using sedimentary paleomarkers, example from the
1297 Gulf of Lion. Earth and Planetary science Letters, 388: 353-366. DOI:
1298 10.1016/j.epsl.2013.11.059.
1299 Reading, H. G., 1991. The classification of deep-Sea depositional systems by sediment
1300 caliber and feeder system. Journal of the Geological Society, 148: 427-430. DOI:
1301 10.1144/gsjgs.148.3.0427.
1302 Schwenk, T., Spiess, V., Breitzke, M. and Hubscher, C., 2005. The architecture and
1303 evolution of the Middle Bengal Fan in vicinity of the active channel-levee system imaged by
1304 high-resolution seismic data. Marine and Petroleum Geology, 22 (5): 637-656. DOI:
1305 10.1016/j.marpetgeo.2005.01.007.
1306 Shaw, J., Puig, P. and Han, G. Q., 2013. Megaflutes in a continental shelf setting, Placentia
1307 Bay, Newfoundland. Geomorphology, 189: 12-25. DOI: 10.1016/j.geomorph.2013.01.010.

1308 Stevenson, C. J., Jackson, C. A. L., Hodgson, D. M., Hubbard, S. M. and Eggenhuisen, J. T.,
1309 2015. Deep-water sediment bypass. Journal of Sedimentary Research, 85 (9): 1058-1081.
1310 DOI: 10.2110/jsr.2015.63.
1311 Straub, K. M. and Pyles, D. R., 2012. Quantifying the hierarchical organization of
1312 compensation in submarine fans using surface statistics. Journal of Sedimentary Research,
1313 82 (11-12): 889-898. DOI: 10.2110/jsr.2012.73.
1314 Sumner, E. J., Talling, P. J., Amy, L. A., Wynn, R. B., Stevenson, C. J. and Frenz, M., 2012.
1315 Facies architecture of individual basin-plain turbidites: Comparison with existing models and
1316 implications for flow processes. Sedimentology, 59 (6): 1850-1887. DOI: 10.1111/j.1365-
1317 3091.2012.01329.x.
1318 Sylvester, Z., Pirmez, C. and Cantelli, A., 2011. A model of submarine channel-levee
1319 evolution based on channel trajectories: Implications for stratigraphic architecture. Marine
1320 and Petroleum Geology, 28 (3): 716-727. DOI: 10.1016/j.marpetgeo.2010.05.012.
1321 Torres, J., 1995. Analyse détaillée du transfert de sédiment du continent vers le bassin : le
1322 Quaternaire terminal au large du Delta du Rhône (Méditerranée nord-occidentale). PhD
1323 Thesis, Brest University (UBO). 353 pp.
1324 Torres, J., Droz, L., Savoye, B., Terentieva, E., Cochonat, P., Kenyon, N. H. and Canals, M.,
1325 1997. Deep-sea avulsion and morphosedimentary evolution of the Rhone Fan Valley and
1326 Neofan during the late Quaternary (north-western Mediterranean Sea). Sedimentology, 44
1327 (3): 457-477. DOI: 10.1046/j.1365-3091.1997.d01-36.x.
1328 Twichell, D. C., Kenyon, N. H., Parson, L. M. and McGregor, B. A., 1991. Depositional
1329 Patterns of the Mississippi Fan Surface: Evidence from GLORIA II and High-Resolution
1330 Seismic Profiles. Seismic Facies and Sedimentary Processes of Submarine Fans and
1331 Turbidite Systems. P. Weimer and M. H. Link. New York, NY, Springer**:** 349-363.
1332 Van der Merwe, W. C., Hodgson, D. M., Brunt, R. L. and Flint, S. S., 2014. Depositional
1333 architecture of sand-attached and sand-detached channel-lobe transition zones on an
1334 exhumed stepped slope mapped over a 2500 km(2) area. Geosphere, 10 (6): 1076-1093.
1335 DOI: 10.1130/ges01035.1.

Wynn, R. B., Kenyon, N. H., Masson, D. G., Stow, D. A. V. and Weaver, P. P. E., 2002a. Characterization and recognition of deep-water channel-lobe transition zones. American Association of Petroleum Geologist Bulletin, 86 (8): 1441-1146. DOI: 10.1306/61EEDCC4-173E-11D7-8645000102C1865D.

Wynn, R. B., Piper, D. J. W. and Gee, M. J. R., 2002b. Generation and migration of coarse-grained sediment waves in turbidity current channels and channel-lobe transition zones. Marine Geology, 192 (1-3): 59-78.

Wynn, R. B. and Stow, D. A. V., 2002. Recognition and interpretation of deep-water sediment waves: implications for palaeoceanography, hydrocarbon exploration and flow process interpretation. Marine Geology, 192 (1-3): 1-3. DOI: 10.1016/S0025-3227(02)00546-7.

Zhang, L. F., Pan, M. and Wang, H. L., 2017. Deepwater turbidite lobe deposits: A review of the research frontiers. Acta Geologica Sinica-English Edition, 91 (1): 283-300. DOI: 10.1111/1755-6724.13078.

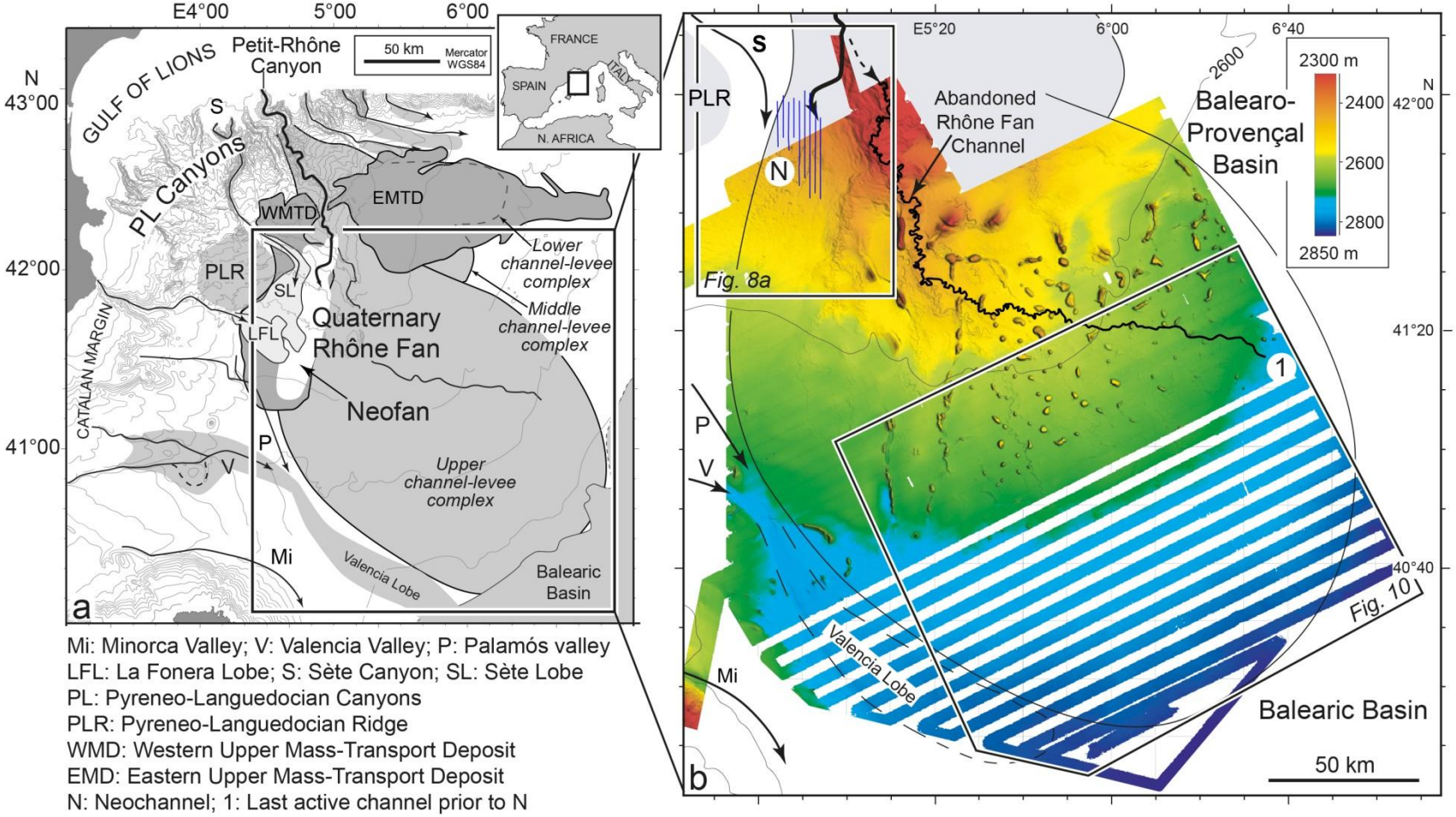

1350

1351 Figure 1

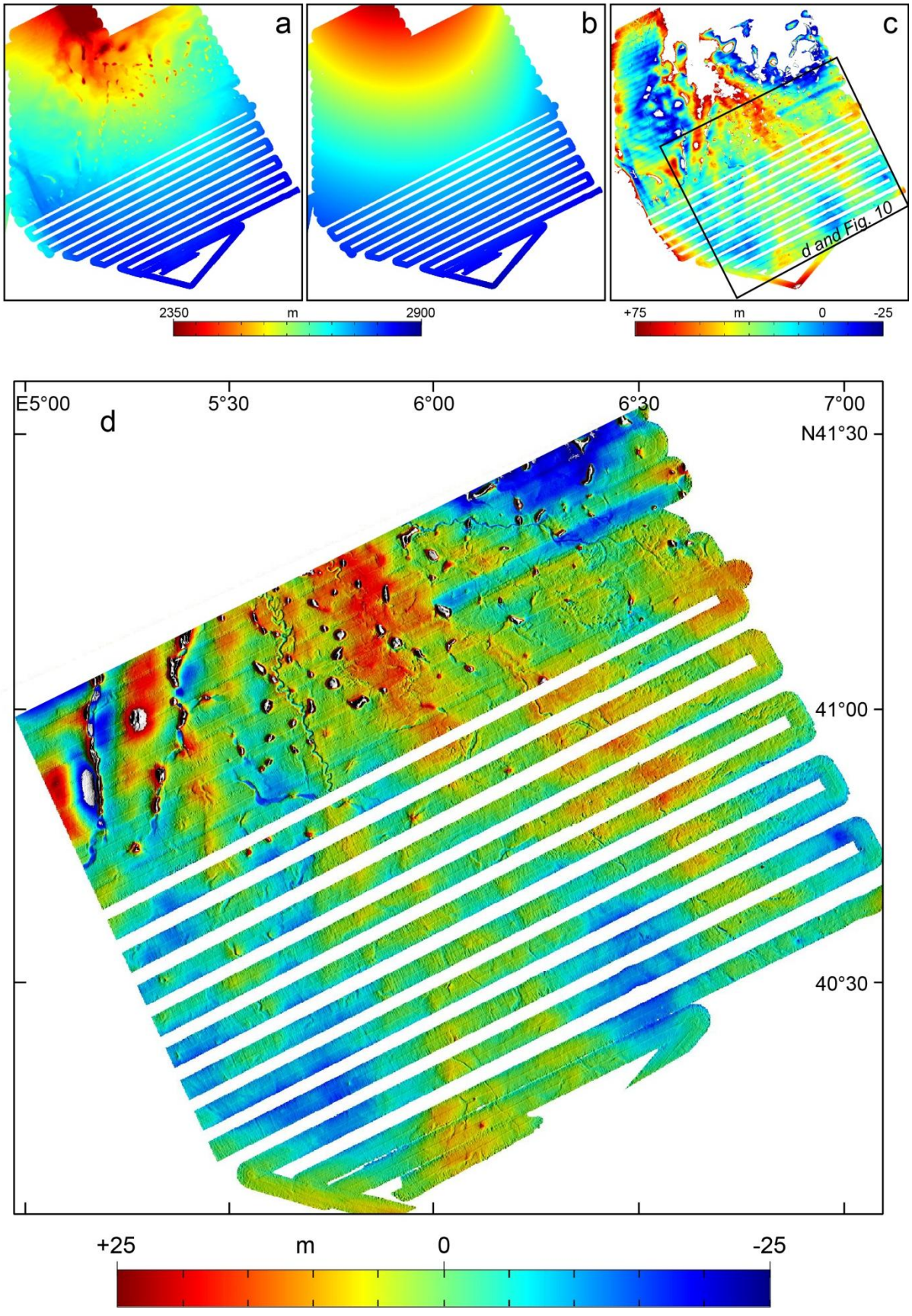

1352

1353 Figure 2

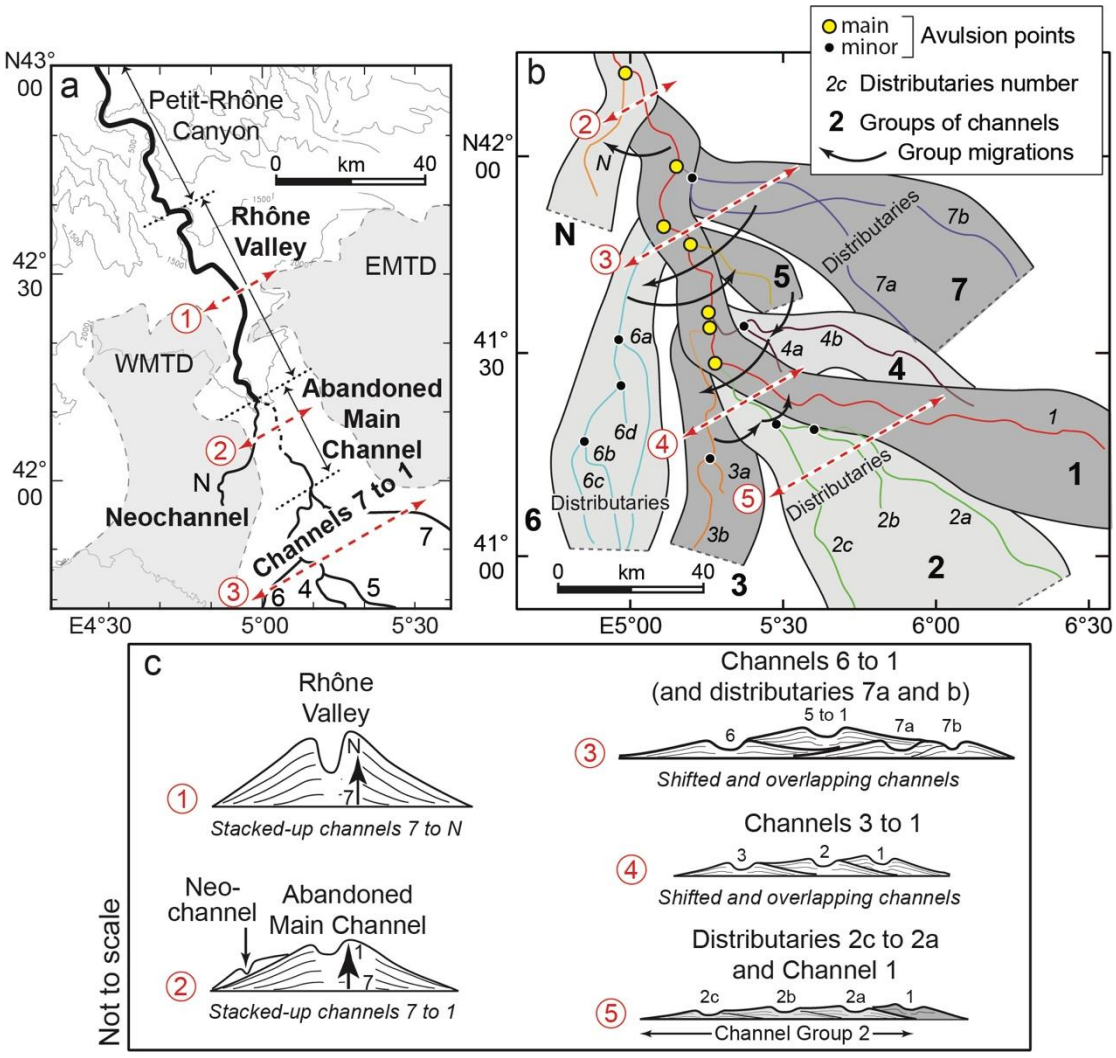

1354

1355 Figure 3

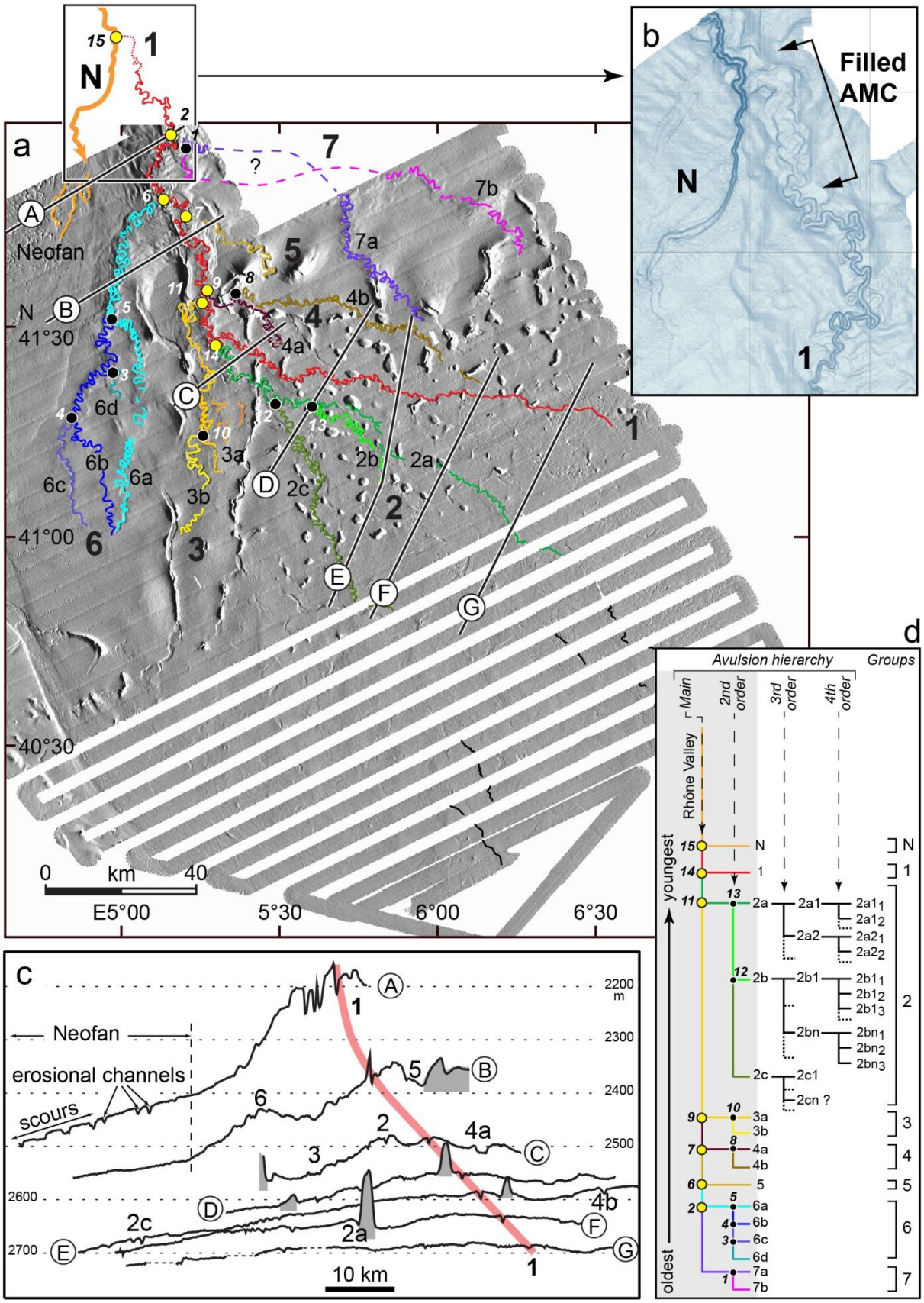

1356

1357 Figure 4

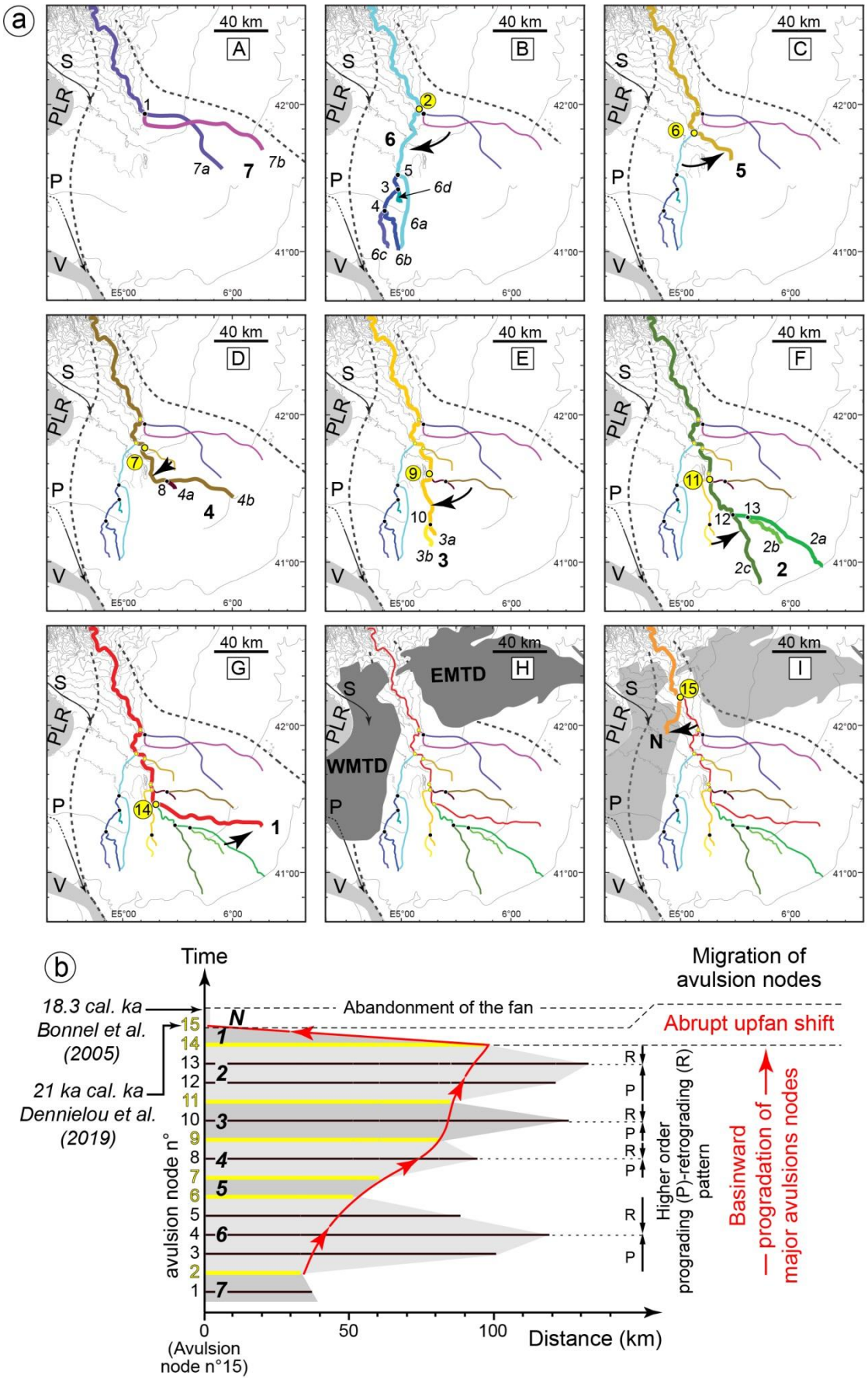
a
40 km
A
B
C
D
E
F
G
H
I
S
PLR
P
V
42°00
41°00
E5°00
6°00
1
7a
7
7b
2
6
5
3
6d
4
6a
6c
6b
5
6
7
8
4a
4
4b
9
10
3a
3b
3
11
13
12
2a
2b
2c
2
14
1
EMTD
WMTD
15
N
b
Time
Migration of avulsion nodes
18.3 cal. ka
Bonnel et al. (2005)
21 ka cal. ka
Dennielou et al. (2019)
Abandonment of the fan
Abrupt upfan shift
avulsion node n°
Higher order prograding (P)-retrograding (R) pattern
Basinward — progradation of — major avulsions nodes
0
50
100
Distance (km)
(Avulsion node n°15)

Figure 5

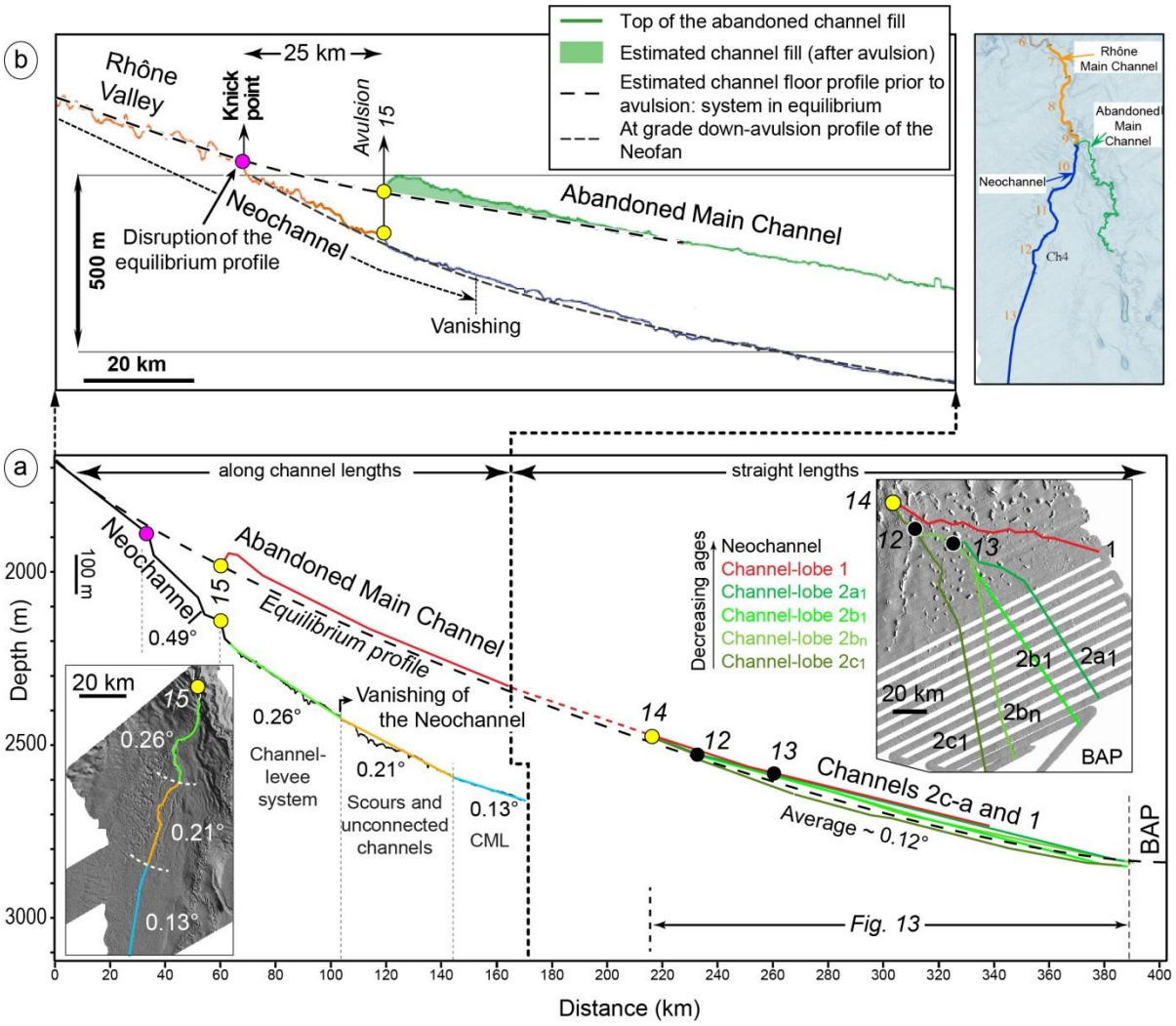

1360

1361 Figure 6

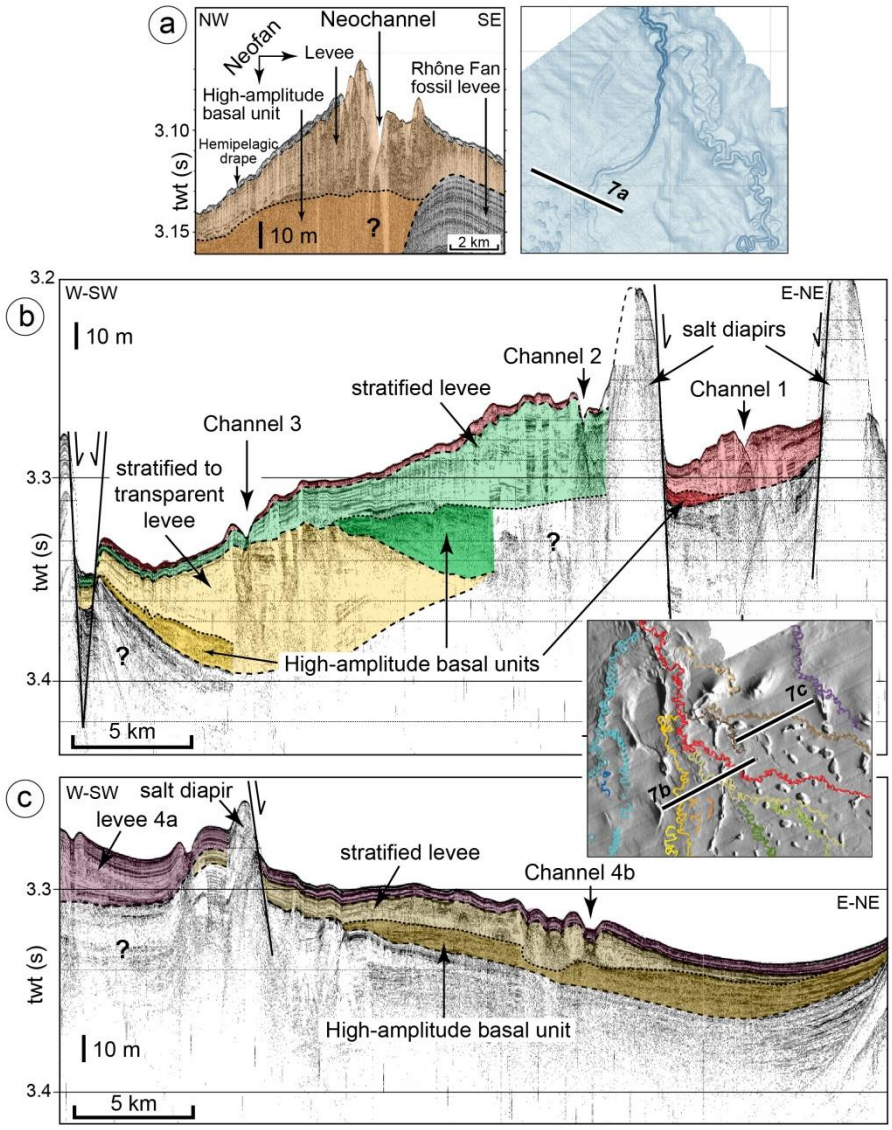
a
NW
SE
Neochannel
Neofan
Levee
Rhône Fan
fossil levee
High-amplitude
basal unit
Hemipelagic
drape
3.10
3.15
twt (s)
10 m
?
2 km
7a
b
W-SW
E-NE
10 m
salt diapirs
Channel 2
Channel 1
stratified levee
Channel 3
stratified to
transparent
levee
3.2
3.3
3.4
twt (s)
?
High-amplitude basal units
5 km
7c
7b
c
W-SW
salt diapir
levee 4a
stratified levee
Channel 4b
E-NE
3.3
3.4
twt (s)
?
10 m
High-amplitude basal unit
5 km

Figure 7

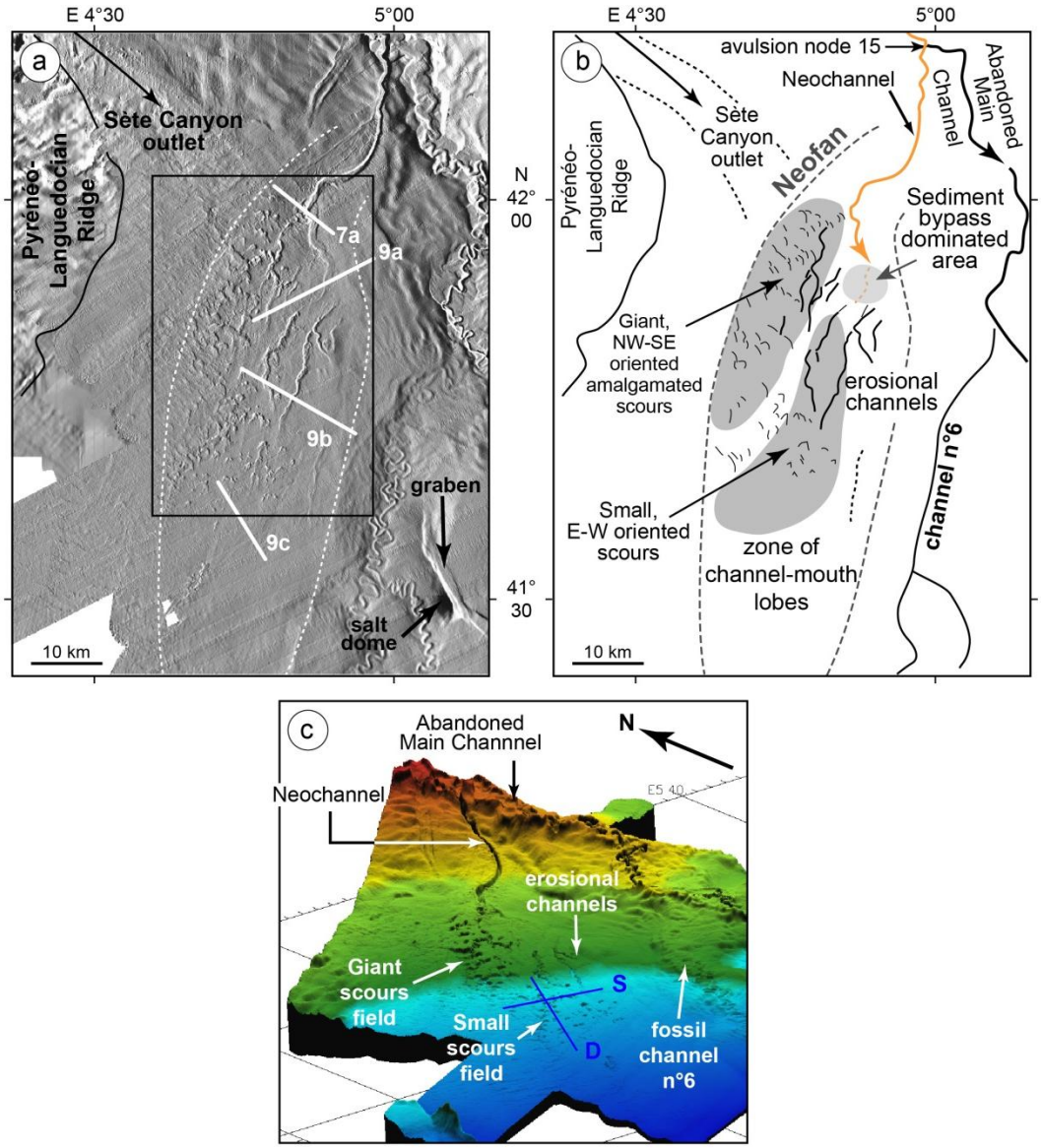

1364

1365 Figure 8

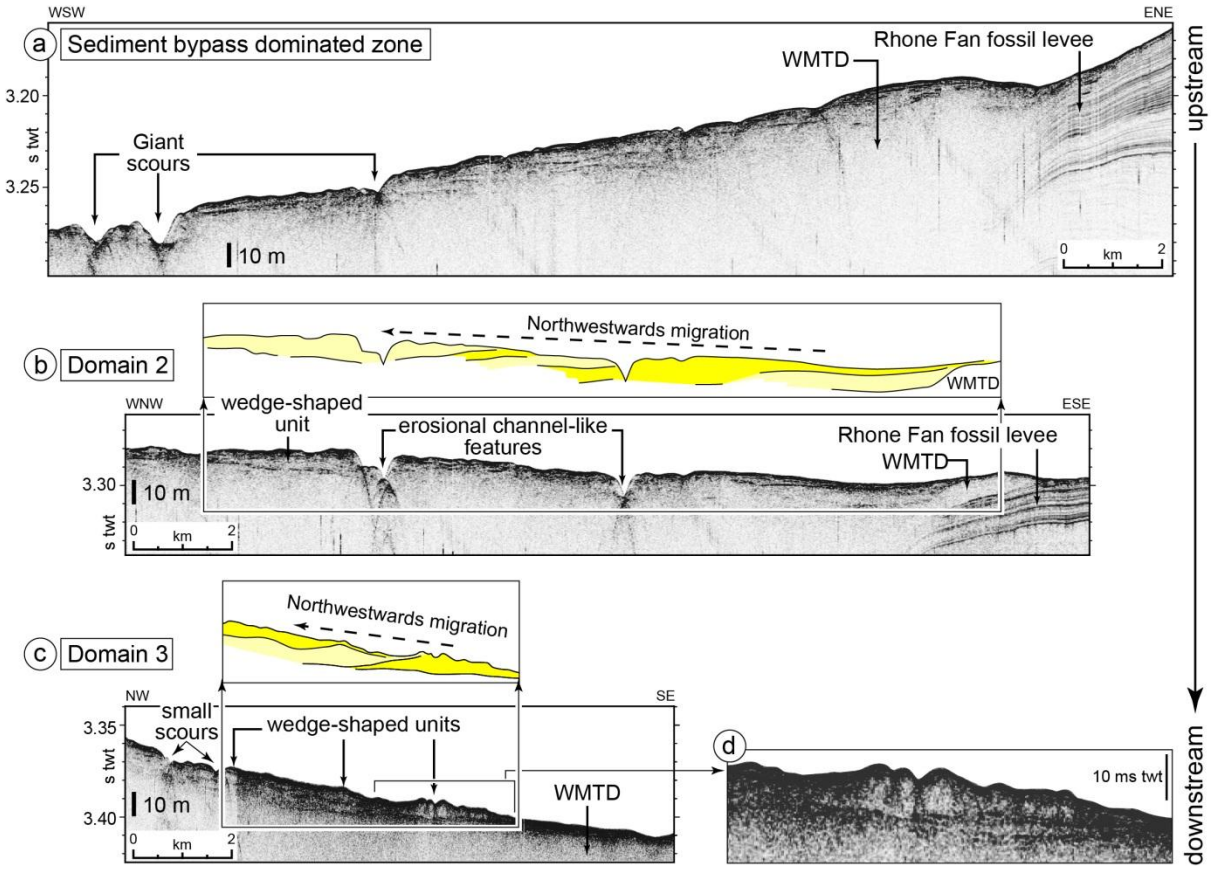

1366

1367 Figure 9

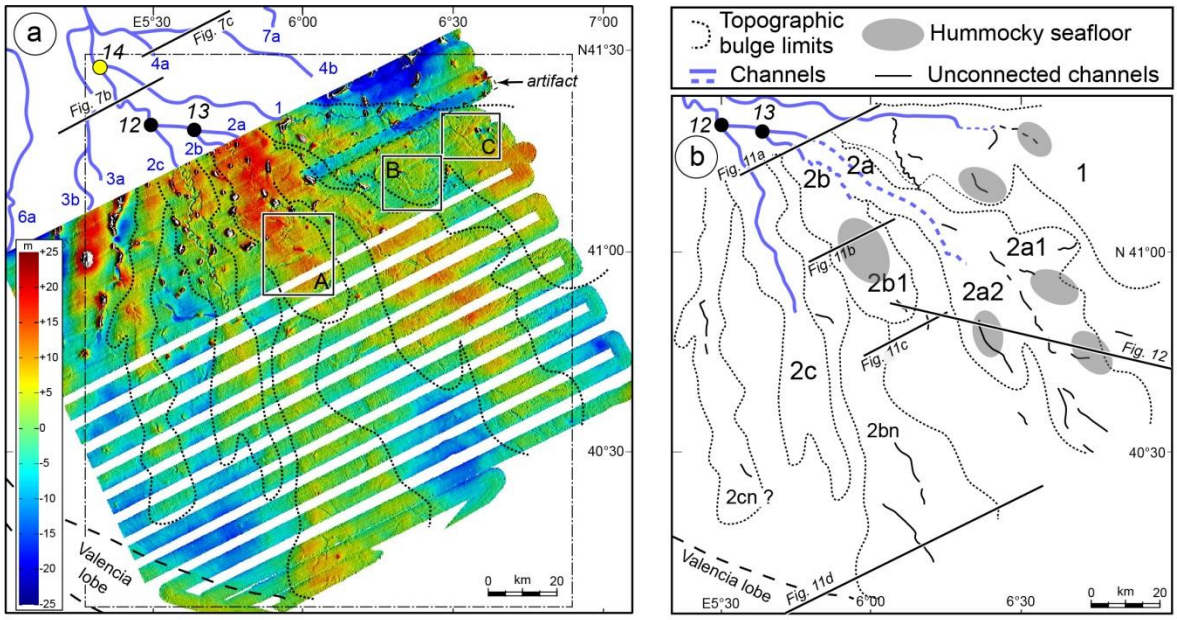
a
E5°30
6°00
6°30
7°00
N41°30
41°00
40°30
Fig. 7c
Fig. 7b
7a
4a
4b
artifact
14
13
12
1
2a
2b
2c
3a
3b
6a
A
B
C
m
+25
+20
+15
+10
+5
0
-5
-10
-15
-20
-25
Valencia lobe
0 km 20
b
Topographic bulge limits
Channels
Hummocky seafloor
Unconnected channels
Fig. 11a
Fig. 11b
Fig. 11c
Fig. 11d
Fig. 12
2b
2a
1
2a1
2b1
2a2
2c
2bn
2cn ?
N 41°00
40°30
E5°30
6°00
6°30
0 km 20

Figure 10

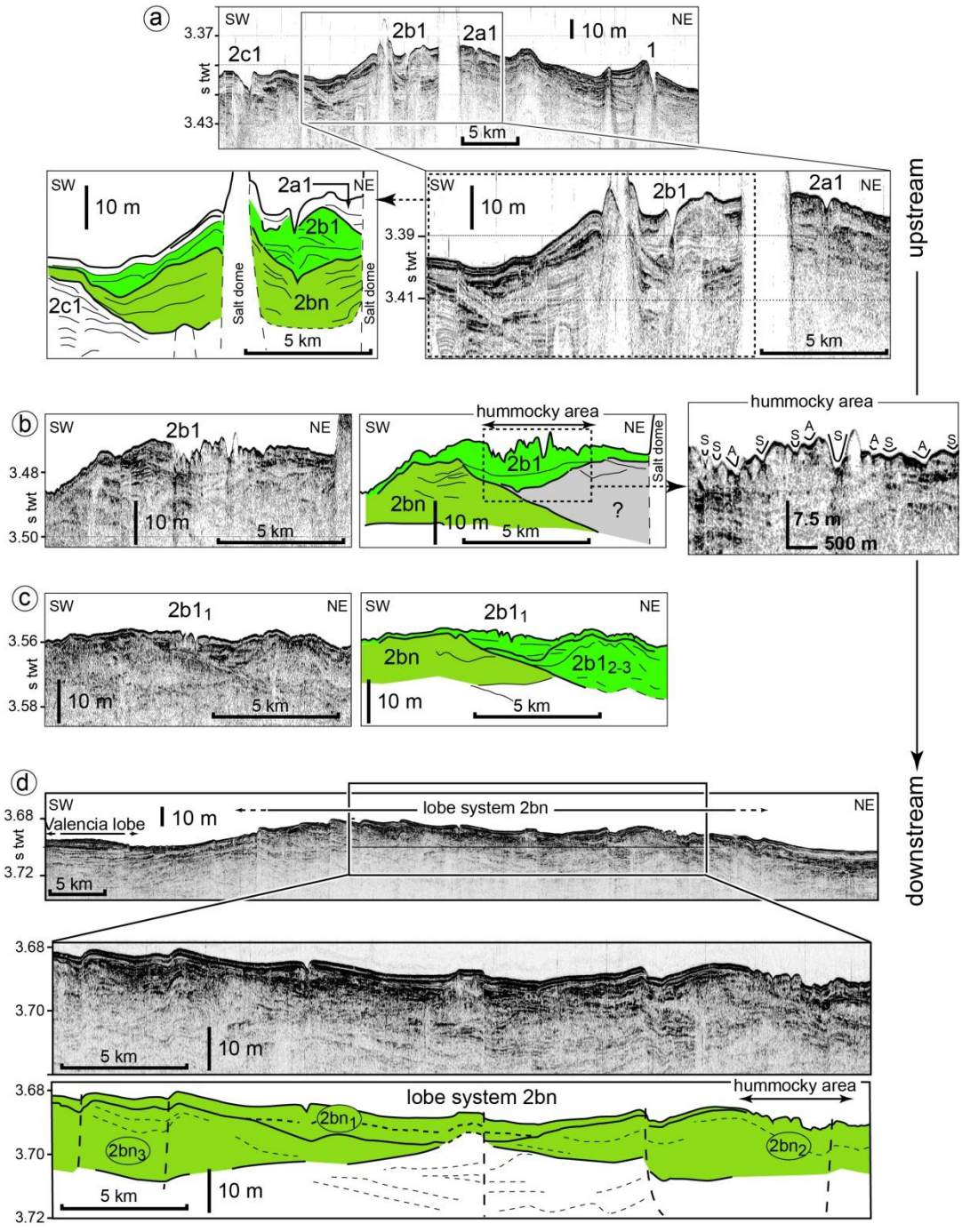

1370

1371 Figure 11

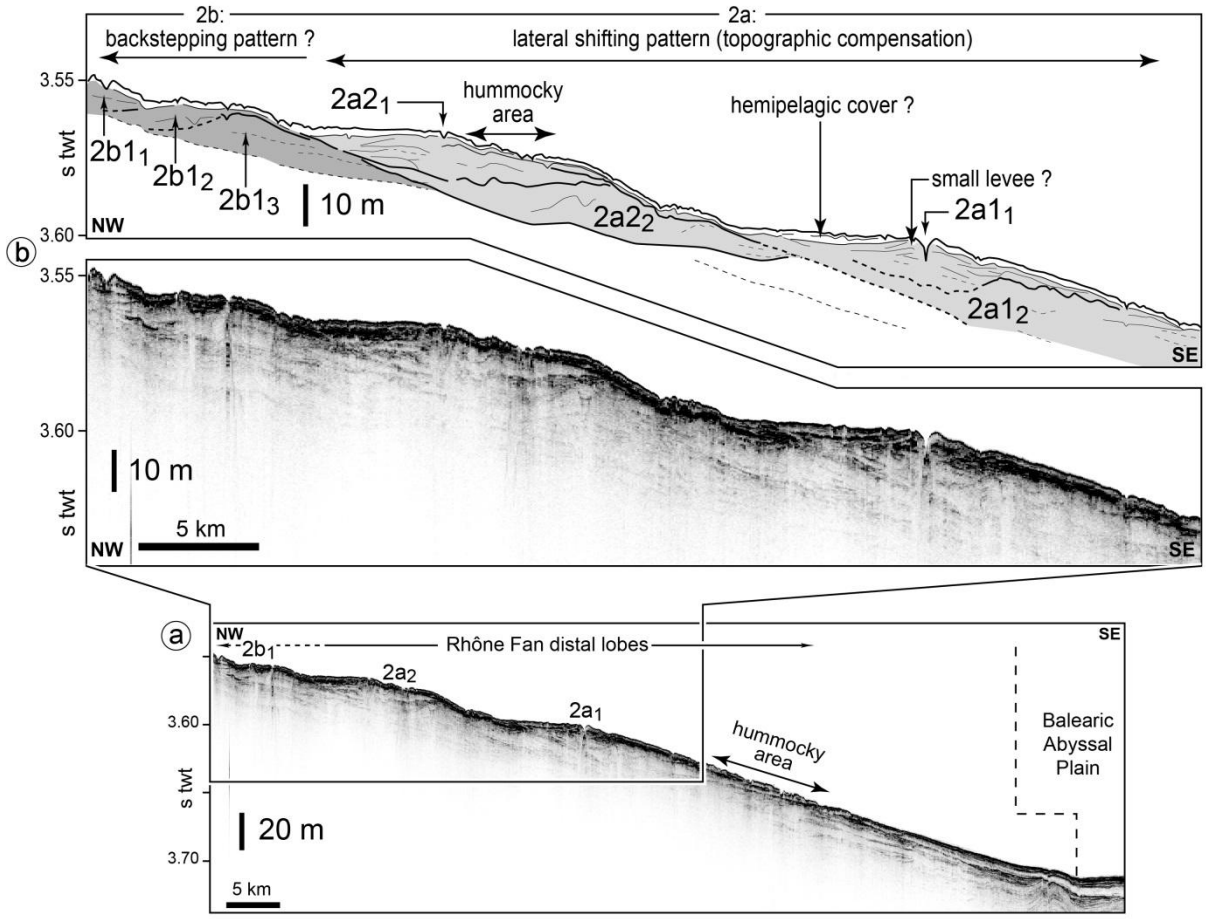

1372

1373 Figure 12

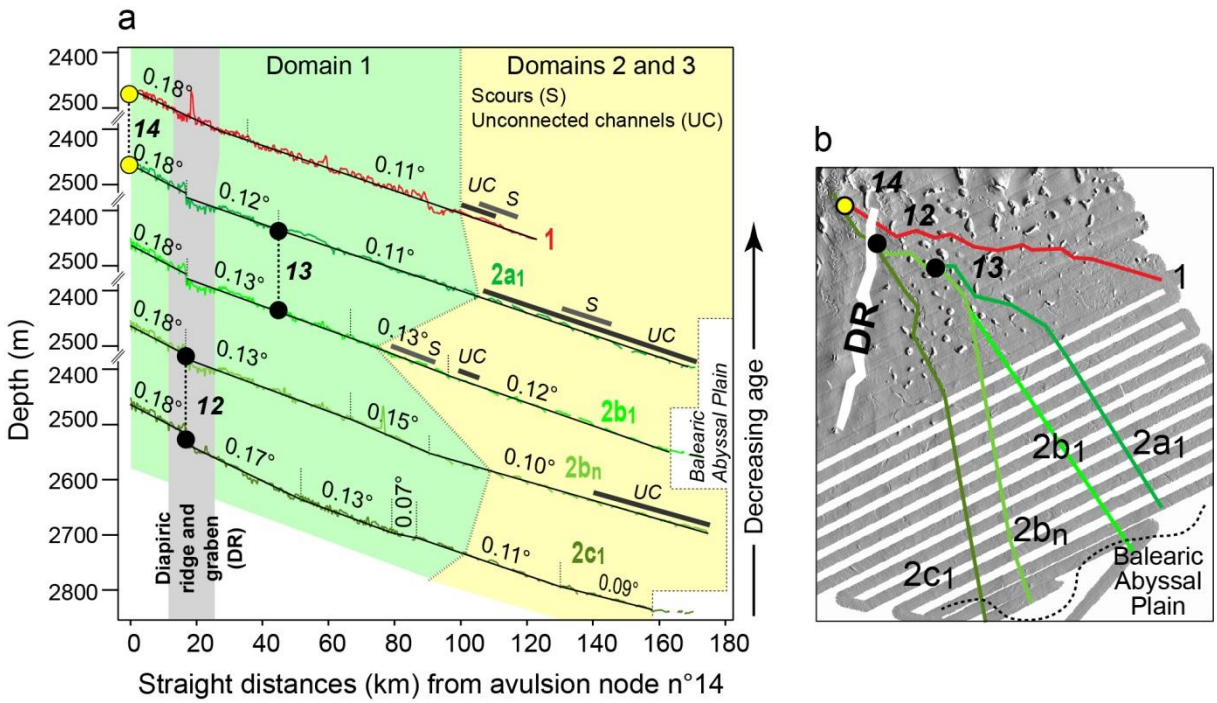

1374

1375 Figure 13

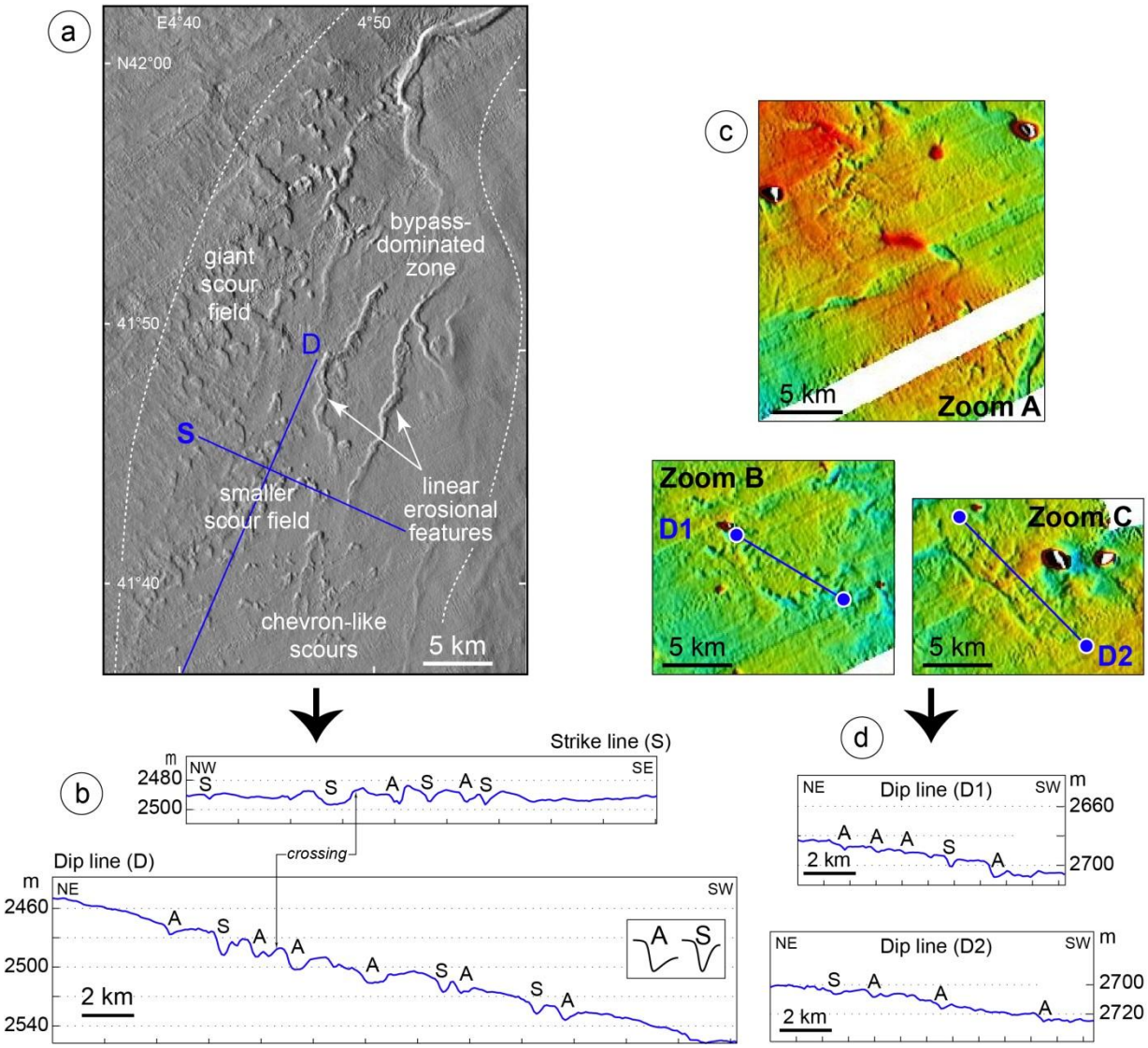

1376

1377 Figure 14

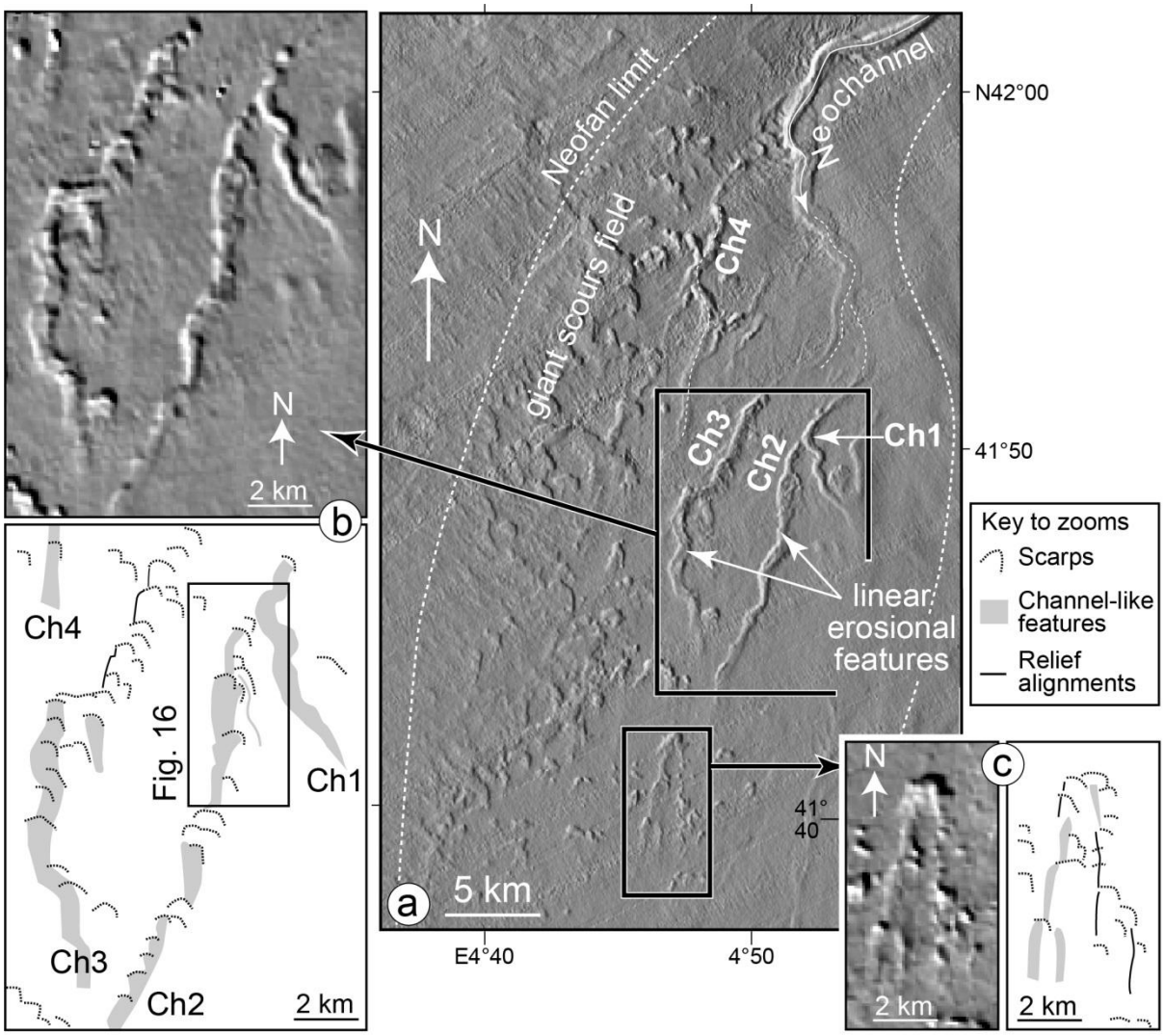

1378

1379 Figure 15

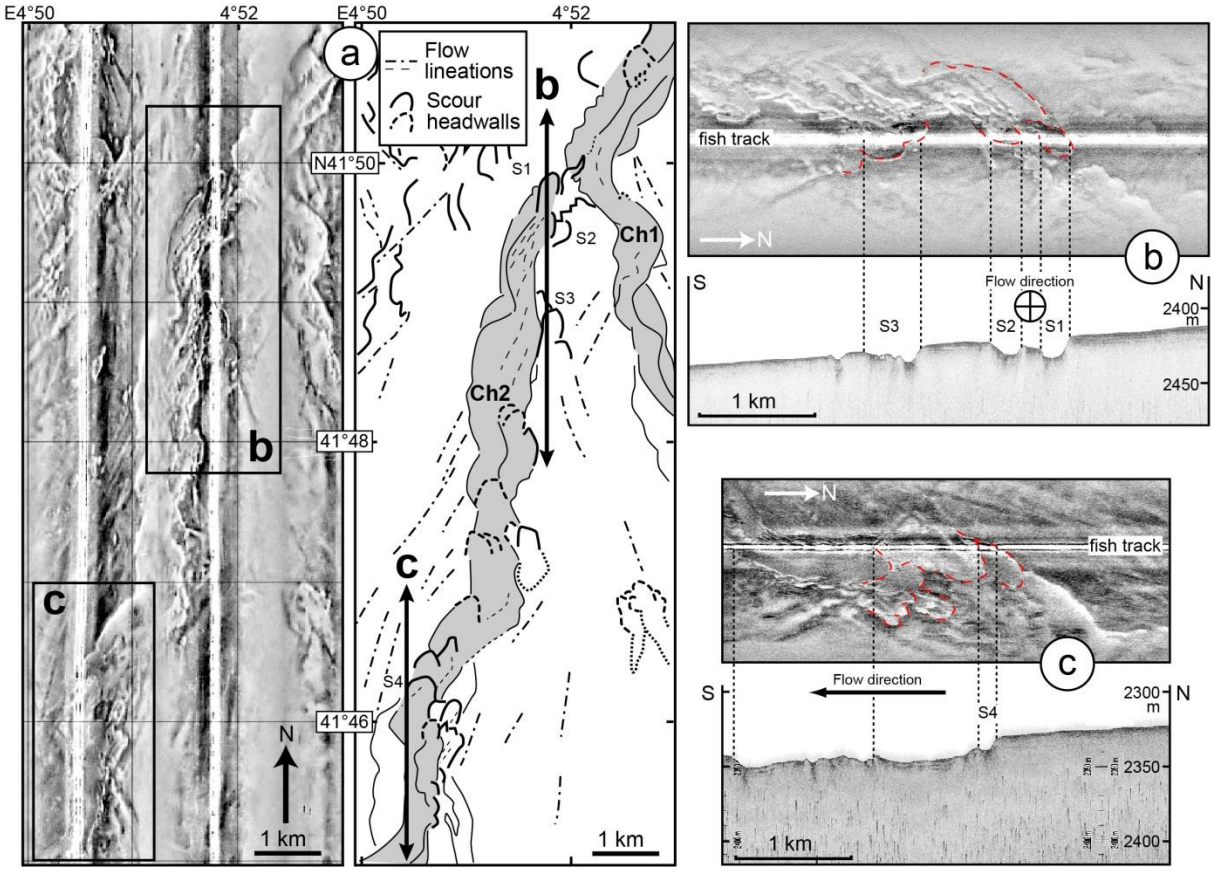

1380

1381 Figure 16

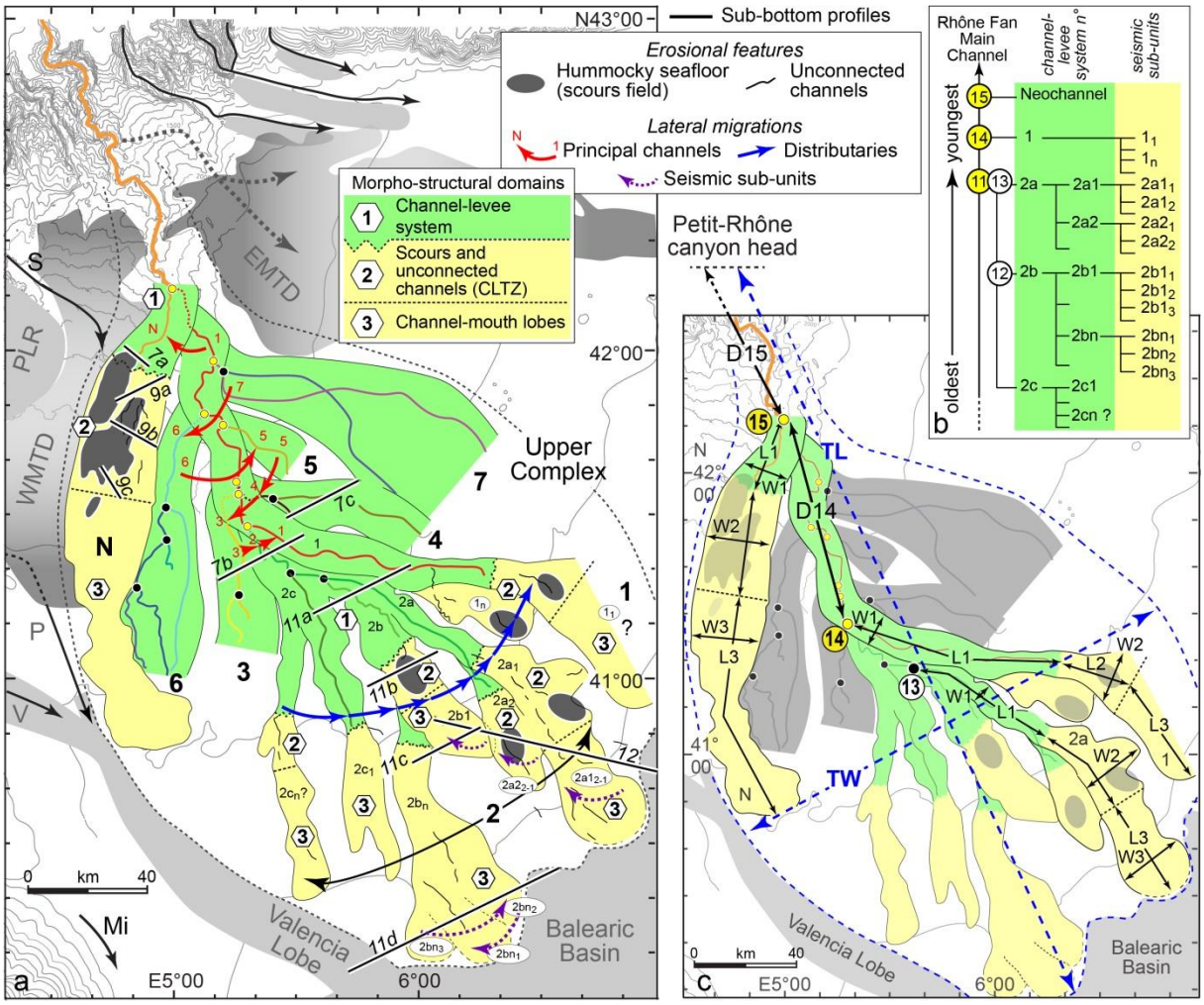

1382

1383 Figure 17

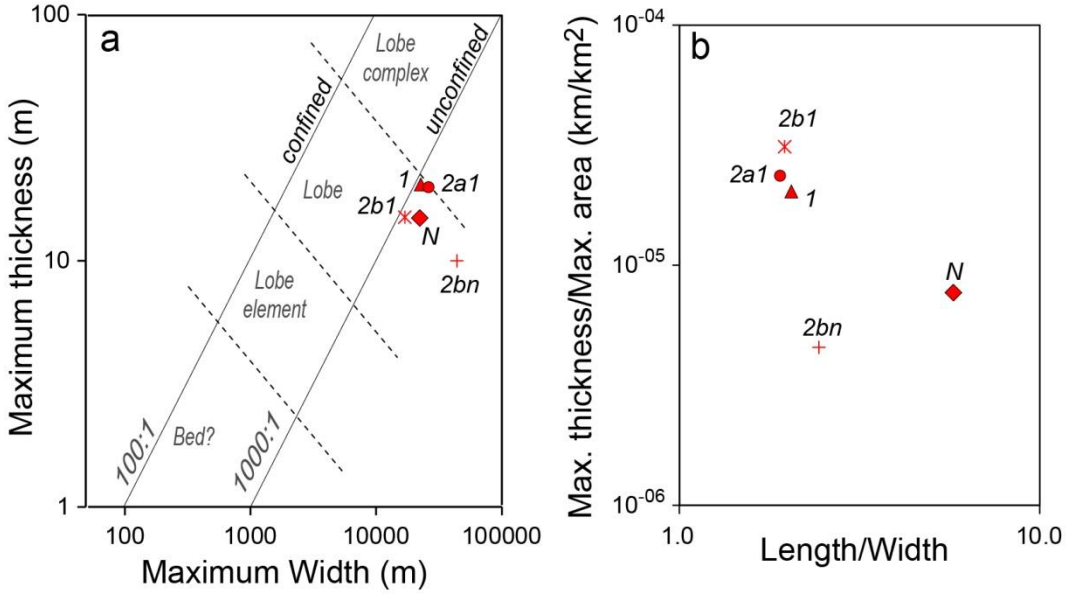

1384

1385 Figure 18

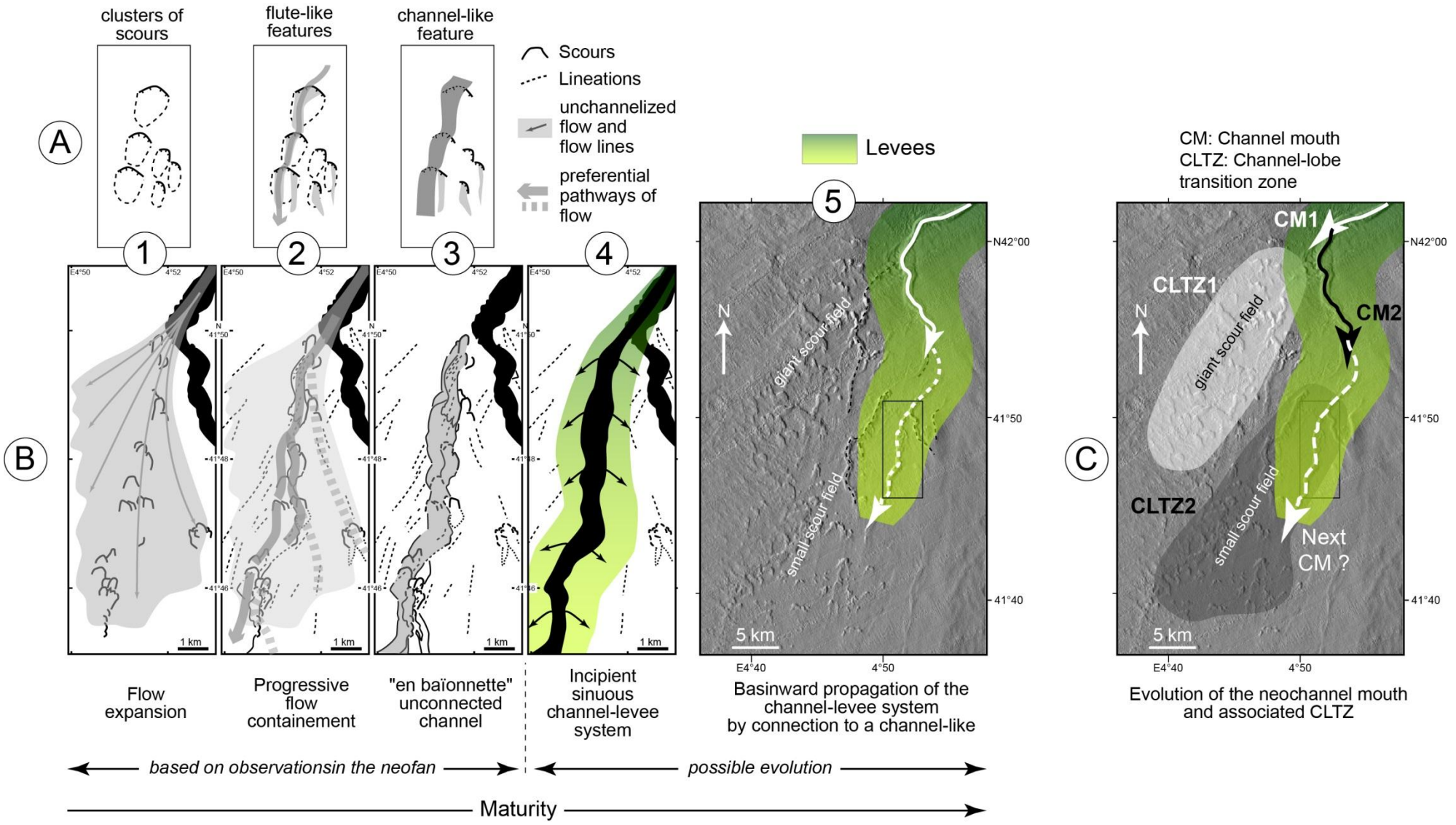

1386

1387 Figure 19

	Late Quaternary Rhône fan (Late Upper Complex)	
Total width (TW, km)	190	
Total length from the canyon head (TL, km)	370	
	Neofan	**2c to 1**
Water depth (m)	2000-2600	2100-2855
Mean slope (°)	0.20	0.12
Age (cal. ka)	21-18.5	> 21
Distance from canyon head to avulsion nodes (km)	D15: 119	D15+D14: 208

1388

1389 Table 1

		Geometry				Scours						Unconnected channels		Wedge-shaped units
						Giant scour field			Small scour field					
CMLs	Domains	Slope (°)	W (km)	L (km)	T (m)	Ds (m)	Ws (km)	Ls (km)	Ds (m)	Ws (km)	Ls (km)	Dc (m)	Lc (km)	Thickness (m)
Neofan	1	0.26	17	29	30	-	-	-	-	-	-	-	-	-
	2	0.21	10 to 29	40	-	10 to 30	1 to 2	1 to 5	5 to 10	< 0.5	0.3*	10	15	-
	3	0.13	22	89	-	-	-	-	-	-	-	-	-	10 to 15* (rarely 45*)
2c to 1	1	0.15 to 0.13	8 to 19	46 to 84	30	-	-	-	-	-	-	-	-	-
	2	0.13 to 0.10	17 to 25	17 to 39	-	-	-	-	5 to 10	0.1 to 0.2	0.6	up to 7	10 to 20	-
	3	~ 0.10	11 to 26	29 to 80	-	-	-	-	-	-	-	-	-	10 to 20

*from Jégou (2008); -: not applicable or unknown; W, L, T: width, length and total thickness; Ds, Ws, Ls: scours depth, width and length, respectively; Dc, Lc: unconnected channels depth and length, respectively.

Table 2

1395